Quaternary Science Reviews
June 2021, Volume 261 Pages 106928 (19p.)
https://doi.org/10.1016/j.quascirev.2021.106928
https://archimer.ifremer.fr/doc/00691/80343/

Post–glacial tephrochronology record off the Chilean continental margin (~41° S)

Fontaine Consuelo Martínez [1, 2, *], Siani Giuseppe [1], Delpech Guillaume [1], Michel Elisabeth [2], Villarosa Gustavo [3], Manssouri Fatima [2], Nouet Julius [1]

[1] Géosciences Paris-Saclay GEOPS/IPSL, UMR CNRS-Université Paris-Saclay 8148, Bat 504 - Université Paris-Saclay, 91405 Orsay Cedex, France
[2] Laboratoire des Sciences du Climat et de l'Environnement LSCE/IPSL, UMR CEA-CNRS-UVSQ 8212, Bat 714 - CEA Saclay, pièce 1034, Site de l'Orme des Merisiers Chemin de Saint Aubin - RD 128, F-91191 Gif sur Yvette Cedex, France
[3] Instituto Patagónico de Tecnologías Biológicas y Geoambientales IPATEC, CONICET-Universidad Nacional Del Comahue, Av De Los Pioneros 2350, 8400, San Carlos de Bariloche, Río Negro, Argentina

* Corresponding author : Consuelo Martinez Fontaine, email address : consuelo.martinez-fontaine@universite-paris-saclay.fr

Abstract :

The Southern Volcanic Zone of the Andes (~33–46° S) is a very active volcanic zone with several volcanic centers recording recurrent historical activity (e.g. Llaima, Villarrica, Puyehue-Cordón Caulle, Osorno, Calbuco and Hudson). Tephrochronology is a valuable tool to help better understand the eruptive history of volcanic centers, essential for producing volcanic hazard maps. Additionally, tephrochronology can also be very useful to synchronize stratigraphic records of different nature such as paleoclimatological, paleoceanographical and archaeological records on land, lakes, ice and the ocean. Here we present a (crypto) tephrochronological record from two marine sediment cores retrieved in the Chilean continental margin at ~41° S and ~41.6° S. The records display continuous sedimentation since the late glacial, as robustly constrained by planktonic foraminifera δ18O and 14C dates. During this period, twenty three cryptotephras were identified as glass shard peaks together with two ~25–30 cm–thick visible tephras (one in each core). The source of the (crypto) tephras was mainly constrained by major and trace element geochemistry of individual glass shards together with their stratigraphic position, since it is not possible to observe physical characteristics, such as color and grain size, when analyzing cryptotephras. From these, one cryptotephra was robustly correlated with the HW7 eruption from the Hudson volcano occurring in the Late Holocene at ~1.5 cal ka BP; and the two visible tephra layers were identified as distant correlatives of the Lepué tephra originating from Michinmahuida volcano and occurring in the Deglaciation/Holocene transition at around 11 cal ka BP. Additionally, eight cryptotephra occurring at ~3.6, 6.2, 7.0, 8.5, 9.6, 14.2, 15.9 and 18.2 cal ka BP were robustly identified as sourced from

Michinmahuida volcano but where otherwise not correlated, providing novel evidence of pre Holocene activity of this volcanic center.

Highlights

► Post–glacial marine tephrochronology record in the Southern Volcanic Zone of the Andes. ► Robust evidence for continuous post–glacial activity of Michinmahuida volcano. ► New explosive evidence for late glacial and deglacial activity in the area.

Keywords : Post-glacial, Quaternary, South America, Southern volcanic zone, Sedimentology-marine cores, Tephrochronology, Radiocarbon, Major and trace elements

1. Introduction

Tephrochronology is a powerful tool not only to unveil the eruptive history of a territory, but to provide a robust chronological framework for its stratigraphic record. By identifying the pyroclastic remains of specific eruptions (tephra) in different sites, the eruptive history of a determined volcanic center can be reconstructed: its recurrence in time, the dispersion of its products and the magnitude of the different eruptive events. At the same time, the remains of the eruptions can be viewed as stratigraphic time markers, which provide regional chronological tie points for different records. When an explosive eruption occurs, the ejected pyroclastic material is deposited in different environments (land, lakes, ice caps, and the ocean) and by identifying its remains, the chronologies of paleoceanographic, paleoclimatological and archaeological records can be aligned, which is crucial when interpreting the evolution of complex systems, such as the climate.

The Southern Volcanic Zones of the Andes (SVZ) is a very active volcanic zone, composed of at least 60 active volcanic centers between 33° S and 46° S (Figure 1), many of which have had recurrent explosive volcanic activity in post–glacial times (~20 cal ka BP), such as Mocho-Choshuenco (Rawson et al., 2015), Chaitén (Alloway et al., 2017b; Amigo et al., 2013; Watt et al., 2013), Hudson (Haberle and Lumley 1998; Naranjo et al., 1993; Naranjo and Stern, 1998; Kratzmann et al., 2008; Carel et al., 2011; Weller et al., 2014; Weller et al., 2015); and/or in historical times, such as Llaima (Naranjo and Moreno, 1991, 2005; Reubi et al., 2011; Schindlbeck et al., 2014), Puyehue-Cordón Caulle (Alloway et al., 2015; Bertrand et al., 2014; Gerlach et al., 1988; Lara et al., 2006; Naranjo et al., 2017; Singer et al., 2008; Villarosa et al., 2006) and Calbuco (Morgado et al., 2019; Romero et al., 2016; Sellés and Moreno, 2011; Watt et al,. 2011b). Since many of these volcanic centers are located nearby populated areas, volcanology together with tephrochronology become key in reconstructing their eruptive history, from which volcanic hazard maps are produced (e.g. Bertin et al., 2018; Moreno and Naranjo, 2002). At the same time, this recurrent explosive volcanic activity, together with the close proximity of the volcanic centers (Figure 1), have produced a continuous and intricate tephrochronological record in the area (Fontijn et al., 2016), which is entangled within stratigraphic records on land, lakes, the ocean, peat bogs, etc. The latter has the potential of providing robust chronologies for paleo environmental records in Patagonia, crucial for understanding the behavior of global-scale climatic features thought to be important factors controlling glacial–interglacial transitions, such as the Southerly Westerly Winds (e.g. Menviel et al., 2018; Toggweiler et al., 2006) and upwelling in the Southern Ocean (e.g. Anderson et al., 2009; Siani et al., 2013).

In the last 40 years, the study of volcanology together with tephrochronology have increased importantly our understanding of the eruptive history of the SVZ since the late glacial period, revealing high recurrence and explosivity of previously thought to be much less active volcanic centers, such as Chaitén (Alloway et al., 2017b; Amigo et al., 2013; Iglesias et al., 2011; Moreno et al., 2014; Watt et al., 2013). However, it has also become apparent that there are still many volcanic centers in the area, such as Yate, Apagado, Hornopirén (Mella, 2008; Watt et al., 2011b), Yanteles and Corcovado (López-Escobar et al., 1993; Naranjo and Stern, 2004) for which the eruptive history is largely unknown. Efforts towards increasing our knowledge of the volcanic activity in the SVZ include undertaking field work in previously relatively less researched areas (Watt et al., 2011a, b) and increasing the research around specific particularly active volcanic centers such as Puyehue-Cordón Caulle (Alloway et al., 2015; Bertrand et al., 2014; Gerlach et al., 1988; Lara et al., 2006; Naranjo et al., 2017; Singer et al., 2008) and Hudson (Kratzmann et al., 2008; Naranjo et al., 1993; Naranjo and Stern, 1998; Weller et al., 2014). Understanding the eruptive history of this area has additionally benefited from the study of records such as peat (e.g. Stern, 2008; Weller et al., 2019), lake (Bertrand et al., 2008; Fontijn et al., 2014; Moreno et al., 2014; Watt et al., 2011b) and marine sediment cores (Carel et al., 2011). These records provide particularly relevant information in areas were the on land record of the eruptions is not available, either because it is of difficult access, it is in a highly vegetated area (such as volcanoes south of ~42° S), or because it has been eroded, for example by the presence of the Patagonian Ice Sheet (PIS), which covered most of the SVZ south of ~38° S during the late glacial period (Davies et al., 2020). Additionally, if continuous sedimentation occurs, paleoenvironmental signals such as palynological or marine isotopic curves can be obtained from lake or sediment cores, which together with ^{14}C ages provide a more comprehensive context in which the tephras were deposited.

Because of the latter, marine sediment cores retrieved in the Chilean continental margin have great potential of providing relevant information to help complete the tephrochronological record in the area. However, as a result of the predominant wind pattern, it is expected that most eruptions leave rather thin ash deposits within marine sediments as opposed to potent tephra layers, which are routinely studied on land. Cryptotephrochronology identifies the remains of past volcanic eruptions which are invisible to the naked eye, and thus can be used to identify the remains of SVZ eruptions in the Chilean continental margin. Here we use both a tephrochronological and cryptotephrochronological approach to find evidence of past volcanic eruptions in two marine sediment cores retrieved in the Chilean continental margin (Figure 1): core MD07-3098 (~40.93° S, ~75.03° W, 3055 m) and core MD07-3100 (~41.60° S, ~74.95° W, 1609 m). Since physical characteristics of tephras such as grain size, thickness and color, cannot be used in the identification of the volcanic source of the cryptotephras, their characterization is based on the geochemical composition (major and trace elements) of individual glass shards together with the stratigraphic position of the cryptotephras, given by planktonic foraminifera $\delta^{18}O$ and ^{14}C ages.

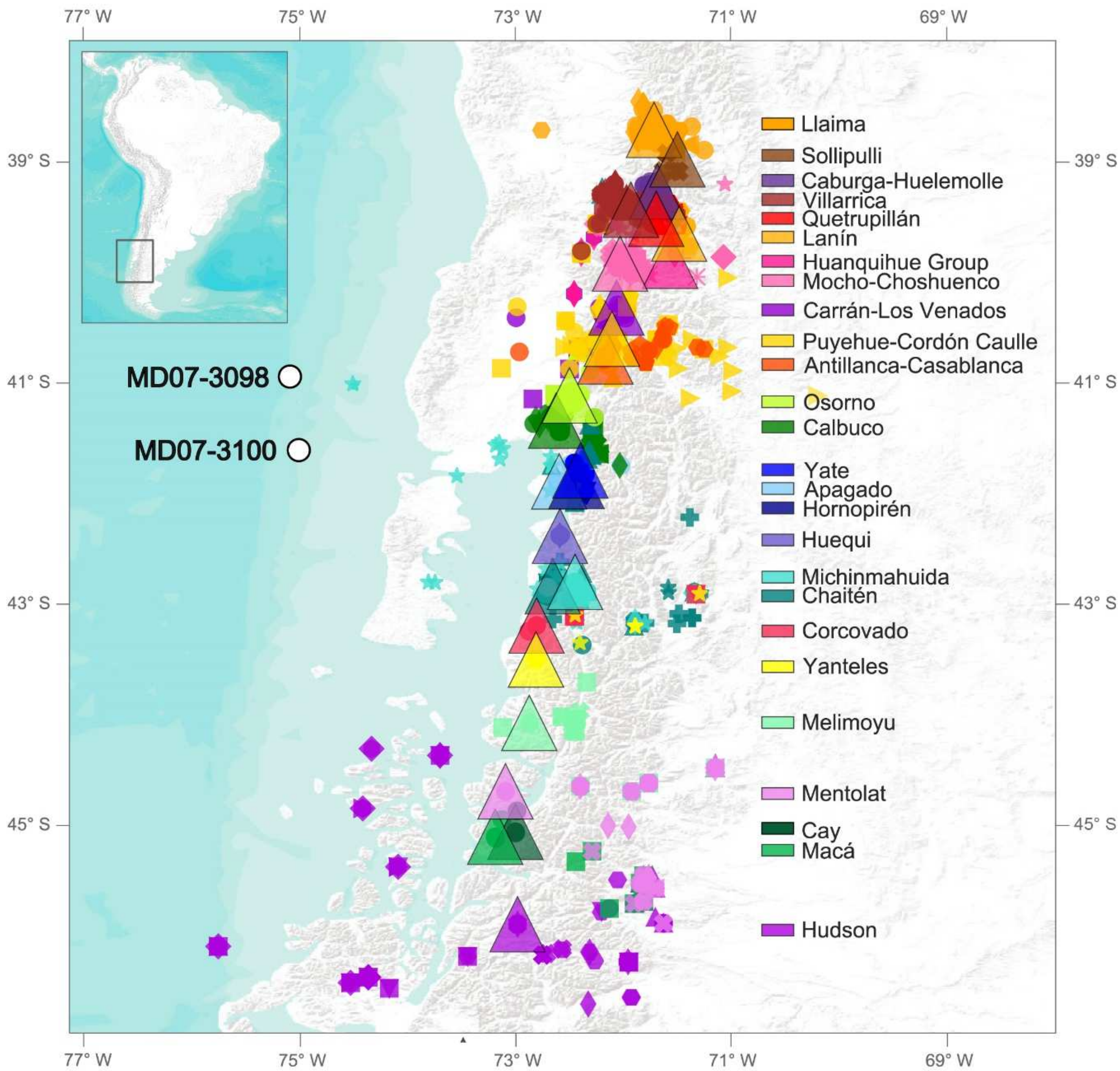

Figure 1. Position of marine sediment cores MD07-3098 (~40.93° S, ~75.03° W, 3055 m) and MD07-3100 (~41.60° S, ~74.95° W, 1609 m), here studied. Additionally, volcanic centers of the Southern Volcanic Zone of the Andes which have been active since at least the late glacial are shown. Only volcanic centers between Llaima and Hudson volcanoes are considered, given the positon of the cores. Also shown are the position of tephrochronological samples which have been analyzed for geochemistry and/or dated. Each volcanic center and associated analyzed sample is assigned a particular color and each eruptive event a particular symbol (detailed legend and references in Figure S16).

2. Volcanological context

The SVZ is one of the four volcanic zones that have been defined in the Andes (Northern (3–6° S), Central (15–27° S), Southern (33–46° S) and Austral (49–55° S); Stern, 2004), which, together with the northern and central zones, derive from the subduction of the Nazca plate under the South American plate. In particular, the SVZ corresponds to the volcanic activity between Tupungatito (~33° S) and Hudson (~46° S) volcanoes, where so far ~60 active volcanic centers have been identified, many of which have recorded recurrent explosive activity in post–glacial times (Global Volcanism Program, Smithsonian Institution. The volcanic products in the SVZ are characterized by a geochemical composition typical of subduction zones: calc–alkaline trends with medium to high–K, relatively high mobile incompatible element concentrations (Cs, Rb, K, Sr, Ba, Pb, Th, U), low REE and HFSE (Zr, Hf, Ta, Nb).

Among the more active and explosive volcanic centers in the area are Puyehue-Cordón Caulle, Calbuco, Michinmahuida and Hudson. Puyehue-Cordón Caulle, situated at ~40.6° S (Figure 1), consists of the Puyehue volcano, which has been active since at least ~300 ka, and the Cordón Caulle fissure, active at least since ~170 ka (Singer et al., 2008). The products from Puyehue-Cordón Caulle range from basaltic to rhyolitic with medium/low–K to medium/high–K affinities (Alloway et al., 2015; Bertrand et al., 2014; Gerlach et al., 1988; Lara et al., 2006; Naranjo et al., 2017; Singer et al., 2008). The most recent explosive events of Puyehue-Cordón Caulle occurred in 1921-1922, 1960 and 2011, the last of which had a Volcanic Explosivity Index (VEI) of 5 (Naranjo et al., 2017), and all of which erupted mainly rhyolitic products. Other eruptive events of similar magnitude have been described in the literature during the Holocene, such as Mil Hojas, Puyehue 2/PCC2 and Puyehue 1/PCC1 (Fontijn et al., 2016; Lara et al., 2006; Naranjo et al., 2017; Singer et al., 2008); and many effusive products corresponding to deglacial times have been dated (Singer et al., 2008) although no explosive correlatives have been identified yet.

The Calbuco volcano, situated at ~41.3° S, has also recorded continuous volcanic activity since around 300 ka (Sellés and Moreno, 2011) and extensive historical activity (e.g. 1792, 1893, 1917, 1929, 1932, 1945, 1961, 1972, 2015) the last of which had a VEI of 4 (Romero et al., 2016). As with Puyehue-Cordón Caulle, Holocene tephras have been more thoroughly described (Watt et al., 2011b), but evidence of explosive activity during the Deglaciation has also been found and dated (Sellés and Moreno, 2011). Most products from Calbuco are andesites or basaltic andesites that have medium to low–K geochemical affinities (López-Escobar et al., 1995, 1992; Sellés and Moreno, 2011).

The Michinmahuida volcano is located at ~42.8° S in a little populated area and has no record of historical activity, however recurrent Holocene activity has been proposed in the literature (Amigo et al., 2013; Moreno et al., 2014). One of the most widespread tephra in the area is associated with Michinmahuida: the Amarillo Ignimbrite, also called the Lepué tephra (Alloway et al., 2017a; Amigo et al., 2013). The eruption that produced this tephra occurred at the beginning of the Holocene (~11 cal ka BP) and erupted bimodal products ranging from basaltic andesites to rhyolites with medium to high–K affinities and has been estimated to have had a VEI of 6 (Amigo et al., 2013).

The Hudson volcano is located at ~46° S in a little populated area difficult to access, as Michinmahuida volcano. Contrastingly, more information can be found about the Hudson volcano than for Michinmahuida, probably because of its highly explosive post–glacial and historical activity, notably, its 1991 eruption with a VEI 4 (Naranjo et al., 1993). Products of Hudson range from basaltic andesites to rhyolites with medium to high–K affinities (Carel et al., 2011; Haberle and Lumley, 1998; Kratzmann et al., 2008; López-Escobar et al., 1993; Naranjo et al., 1993; Naranjo and Stern, 1998; Weller et al., 2014, 2015) and at least 8 tephras have been described and dated in the literature (Ho, HW1, HW2, HW3, H1, H2, HW6 and HW7), the oldest one: Ho, occurred around ~17 cal ka BP with an estimated VEI of 6 and has been identified as far as ~900 km SE of the volcano (Weller et al., 2014).

The presence of the cryptotephra layers in marine cores, retrieved west of the volcanic centers can be somewhat counterintuitive because the dispersion of volcanic ash in the SVZ is largely controlled by the prevailing Southerly Westerly Winds in the area. From what is observed in the literature, but also in modern eruptions such as Chaitén, 2008 (Watt et al., 2009) and Puyehue Cordón Caulle, 2011 (Bertrand et al., 2014), most of the ash produced by explosive eruptions in the central (37–42° S) and southern (42–46° S) zones of the SVZ are transported to the east by the Southerly Westerly Winds, the Subtropical jet and/or the Polar Front Jet (Gallego et al., 2005; Rahn and Garreaud, 2014). A lesser amount of the eruptions record a predominantly northward dispersion, which is associated with the southeast Pacific subtropical anticyclone transporting ashes to the north (Rahn and Garreaud, 2014). Among these, Cha1 from Chaitén (Watt et al., 2013; Fontijn et al., 2016), Neltume from Mocho-Choshuenco (Fontijn et al., 2016; Rawson et al., 2015) and the

Hudson eruption in 1991 (Naranjo et al., 1993). Less frequently, winds to the south and to the west also occur as part of smaller scale phenomena, such as low pressure systems and changes associated to the Southern Hemisphere's baroclinic annular mode (Pérez-Santos et al., 2019), for example during the 2015 eruption of Calbuco (Romero et al., 2016). The latter might explain the less common occurrence of tephra deposits to the west and northwest of volcanoes, such as HW1–7 (Haberle and Lumley, 1998) and Lepué Tephra (Alloway et al., 2017a). Thus, even though ash transported by these short–lived wind directions might not be enough to deposit potent tephra in the ocean in most cases, they are enough to deposit thin ash layers and thus leave traces of past volcanic eruptions identifiable via cryptotephrochronology.

3. Methods

3.1 Core retrieving

Marine sediment cores MD07-3098 (~40.93° S, ~75.03° W, 3055 m) and MD07-3100 (~41.60° S, ~74.95° W, 1609 m) are two CALYPSO cores retrieved by the French R/V Marion Dufresne during the PACHIDERME expedition in February 2007 (Kissel and The Shipboard Scientific Party, 2007). MD07-3098 is a 20.74 m long core composed mainly of silty clay with silty and sandy layers horizons, which also contains a visible tephra layer of ~30 cm between ~7.6–8 m labeled T6/98. MD07-3100 is a 29.8 m long core composed mainly of homogenous silty clays, which displays a visible tephra layer of ~25 cm between 7.25–7.5 m labeled T8/100. For this study, the first 13.5 m and 15 m from core MD07-3098 and MD07-3100 (respectively) have been analyzed, which correspond to the post–glacial portion of these sedimentary archives. Because of the difference in lithology given by the presence of the tephra, both cores present a ~25 cm gap in the upper part of the visible tephra (Figure 2), which are corrected for in the age models.

3.2 Stable isotope stratigraphy

The stratigraphic constraint of the cores is provided by stable oxygen isotope data ($\delta^{18}O$) measured in planktonic foraminifera at the Laboratoire des Sciences du Climat et l'Environnement (LSCE) on Optima VG, GV Isoprime and Finnigan Delta + mass spectrometers. Isotopic measurements were made every 10 cm in one to thirty specimens of planktonic foramininfera *G. bulloides* (250–315 μm fraction) in both cores. This information allowed for a first order identification of the timeframe the cores span (Figure 2). The measurements stopped where a stable late glacial isotopic signal was reached, at ~13.5 m in core MD07-3098 and ~15 m in core MD07-3100. Results from core MD07-3100 have already been published by Haddam et al. (2018) and those for core MD07-3098 are displayed in Table S1.

3.3 Tephra and Cryptotephra identification

Cryptotephra layers were identified as peaks in the relative amount of glass shards and micro–pumice. The cores were sampled every 10 cm in 4 cc box samples, washed, sieved for the fraction>40 μm and rinsed in a 10% HCl solution to dilute the carbonated fraction and allow for the identification only of the detrital fraction. The percentage of glass shards and micro–pumice was obtained by counting the relative amount of glass shards, micro–pumice, crystals, lithics and other detrital material in the detrital fraction >40 μm in at least

300 particles per sample. Primary glass shards and micro–pumice were identified as having pristine angular morphologies with fragile tips and no remineralization coatings (Figure S1). In most depths glass shards color range from a brown-honey color to white, with diverse degrees of vesicularity. The glass shard and micro–pumice peaks were considered where the percentage exceeded the background value at least three times. For core MD07-3100, 115 samples were counted each 10 cm between 60 and 1220 cm, the background was around 5% and sixteen glass shard and micro–pumice peaks were identified as cryptotephras and analyzed for geochemistry with peak values between 15 and 45%. For core MD07-3098, 86 samples were counted with a resolution between 10 and 20 cm, from 1 to 1321 cm depth, the background was 6% and seven glass shard peaks were identified as cryptotephras and analyzed for geochemistry with peak values between 18 and 27%.

In both cores, the visible tephras are recognized by an important change in lithology easily recognizable as a change from olive brown silty clay to black sand (Figure 2). Both tephras present a sharp erosive contact at the base and graded at the top. Because of the graded upper contact, the upper limit of the tephras were identified as an important drop in the glass shard and micro–pumice count in both cores. Additionally, as mentioned in section 3.1, both cores present a gap in the upper part of the tephra deposits, thus the thickness of each tephra is estimated as the sum of the thickness above and below each gap.

3.4 Geochemistry

In order to characterize the geochemistry of the cryptotephras and visible tephras, individual glass shards from the identified layers were hand–picked and mounted in epoxy resin beads and polished on an automated polish wheel to avoid compositional variations due to surficial alteration processes. Major element where determined for each individual glass shard with a CAMECA-SX 100 Electron Microprobe (EPMA-CAMPARIS) at the University Paris VI (France). Ten elements were analyzed (Na, Mg, Si, Al, Cl, K, Ca, Ti, Mn and Fe) using an accelerating voltage of 15 KV, a current of 10 nA and a beam size of 5 µm to minimize loss of alkalis such as Na and the results are presented in Table S2. The instrument calibration was done using natural mineral standards (e.g. Na is calibrated from albite, K from Orthose, Si, Ca and Mg from diopside, Fe from hematite). Precisions on individual shards (1σ) were better than 0.6% for Si, ~1% for Al, 3% for Ca and Mg, 4% for Na, 5% for Fe, 6% for K, 10% for Ti and about 30% for Cl and Mn. The in-house glass standard Lipari was also analyzed as an unknown sample during the analytical sessions (Table S4) and display comparable values to published data (Jochum et al., 2007). As seen on Figure S1, glass shards from different cryptotephra layers and even in a single layer (T8/100) might have very different aspects, such as highly vesiculated and microlite–rich glass shards coexist with non–vesiculated microlite–poor glass shards. Attention was paid to analyze glass shards with the less microlites possible and between ~10 and 30 analyses were acquired for each cryptotephra. Major element data obtained here, as well as those from the literature, were normalized to 100% before plotting in order to being able to compare the analyses.

Additionally, trace element concentrations were measured in ten of the sixteen depths in core MD07-3100 with a Laser Ablation High Resolution ICP-MS (LA-HR-ICPMS) at GEOPS laboratory (Paris-Saclay University). Results are presented in Table S2. For the ablation, a CETAC-Teledyne Excimer 193 nm laser system was connected to an Element XR HR-ICP-MS and the sample was transported to the torch using He gas. A frequency of 5Hz and a fluence of 3.65 J/cm^2, for a spot size of 40 microns were used during analyses. The instrument was calibrated using the international glass standard NIST 612 as an external standard. In order to cover the large range of silica contents determined by EMPA for the glass shards, international glass standards of rhyolitic (ATHO-G; 75.6 wt.% SiO_2) or basaltic (KL2-G; 50.3 wt.% SiO_2) compositions were also run as unknown samples to control the quality of the measurements (Table S4). The reported values in Table S4 compare well with the preferred values from GEOREM (Jochum et al., 2007). For the purpose of the study, internal standards KL2-G and ATHO-G gave a precision (1σ) on La between 2.4 and 3.7%, between 2.7 and 5.2% for Yb, between 3.2 and 3.7% for Zr and between 2 and 2.5% for Nb (Table S4).

3.5 Radiocarbon dating

After identifying the glass shard and micro–pumice peaks, planktonic foraminifera were picked either at the base or in the middle of the peak, according to foraminifera peak abundances. Radiocarbon dates for core MD07-3100 are published in Haddam et al. (2018) whereas new radiocarbon dates for core MD07-3098 are presented in Table S5. Either mono specific *G. bulloides* or mixed planktonic foraminifera were picked from the >150 µm fraction, samples >3 mg were measured at UMS-ARTEMIS (Pelletron 3 MV) AMS facilities (CNRS-CEA Saclay, France, Dumoulin et al., 2017; Moreau et al., 2013), whereas samples <3 mg were analyzed on the gas ion source ECHoMICADAS at the LSCE (Gif-Sur-Yvette, France) using coupling of cracker system to the gas handling system (Wacker et al., 2013; Tisnérat-Laborde et al., 2015). ^{14}C results are reported in conventional age BP according to the convention of Stuiver and Polach (1977), normalized to the base of $\delta^{13}C$ of –25.0‰ relative to the Pee Dee Belemnite (PDB) international standard, and corrected by the age of the background subtraction. The age model for the cores was then obtained with the software Undatable (Lougheed and Obrochta, 2019) with a depth uncertainty of 1 cm, corresponding to the sampling width, and calibrating according to SHCal20 curve (Hogg et al., 2020).

4. Results

4.1 Chronological framework

The obtained stable isotope stratigraphy (Table S1, Figure 2) reveals that both studied cores cover at least the time interval between the late glacial and the Late Holocene and register similar variations and sedimentation rates since. The MD07-3100 $\delta^{18}O$ record displays steady values around 2.7 ‰ between ~12.5–15 m, which characterizes the late glacial in the core (Figure 2). A deglacial decreasing trend is observed between ~12.5–7.5 m, when values decrease from ~2.7 to ~0.9‰ interrupted by two plateaus: around ~11 m and ~8–10 m. Minimum values of ~0.9‰ PDB are reached at ~7.5 m, coincident with the occurrence of the ~25 cm visible tephra (T8/100). Values characteristic of the Holocene are observed between ~7.5 m and the top. In particular: around 7 m $\delta^{18}O$ values reach its mean global minimum of around 0.9‰, followed by a steady increase until 2‰ between 6 and 5 m and finally, between ~5–0 m somewhat steady values of around 1.6‰ occur, with two intervals of lower values between ~3.6–4 and ~0.7–1 m.

The late glacial is observed in core MD07-3098 between ~13.5–11.7 m with steady values around 3‰ (Figure 2). A deglacial decrease is observed between ~11.7–8.1 m. Between

~11.7–10.2 m values decrease until 1.5‰, a slight increase until 1.6‰ is observed between ~10.2–9 m, followed by a steady decrease until reaching minimum values of ~0.9‰ at 8.1 m, coincident with the presence of a ~30 cm thick tephra layer (T6/98). Minimum values of ~0.9‰ maintain until 6.6 m. Between ~6.6–5.6 m, values steadily increase until ~1.8‰ and are maintained at this value until ~3.2 m. From ~3.2 m to the core top values are relatively lighter and more variable.

The age model of core MD07-3098 was obtained from 27 planktonic ^{14}C ages (Table S5, Figure S3), corrected by a mobile marine surface reservoir age (Rs), following the method by Haddam et al. (2018) for core MD07-3100. The similarity of the $\delta^{18}O$ curves of both cores versus their planktonic ^{14}C age (Figure S2) suggests that they record variations of the same water mass (Subantarctic Water) in the studied time interval. Thus, we apply the same Rs correction used for MD07-3100 by Haddam et al. (2018) to the planktonic ^{14}C ages from core MD07-3098 (Table S5). The conventional radiocarbon ages were subsequently calibrated according to the SHCal20 curve (Hogg et al., 2020) and the age model was obtained with the software Undatable (Lougheed and Obrochta, 2019).

From the resulting age model (Table S1, Figure S3, S4), core MD07-3098 has relatively high and nearly constant sedimentation rates during the Holocene and Deglaciation of ~70 cm/ky. Core MD07-3100 has nearly constant sedimentation rates of ~65 cm/ky during the whole studied interval (Haddam et al., 2018). The age model together with the stable isotope stratigraphy indicate that in the studied cores, the late glacial ends between 17–16.5 cal ka BP (Figure S4), the Deglaciation occurs between ~17–16.5 and ~10.5 cal ka BP and the Holocene between ~10.5 cal ka BP and the present.

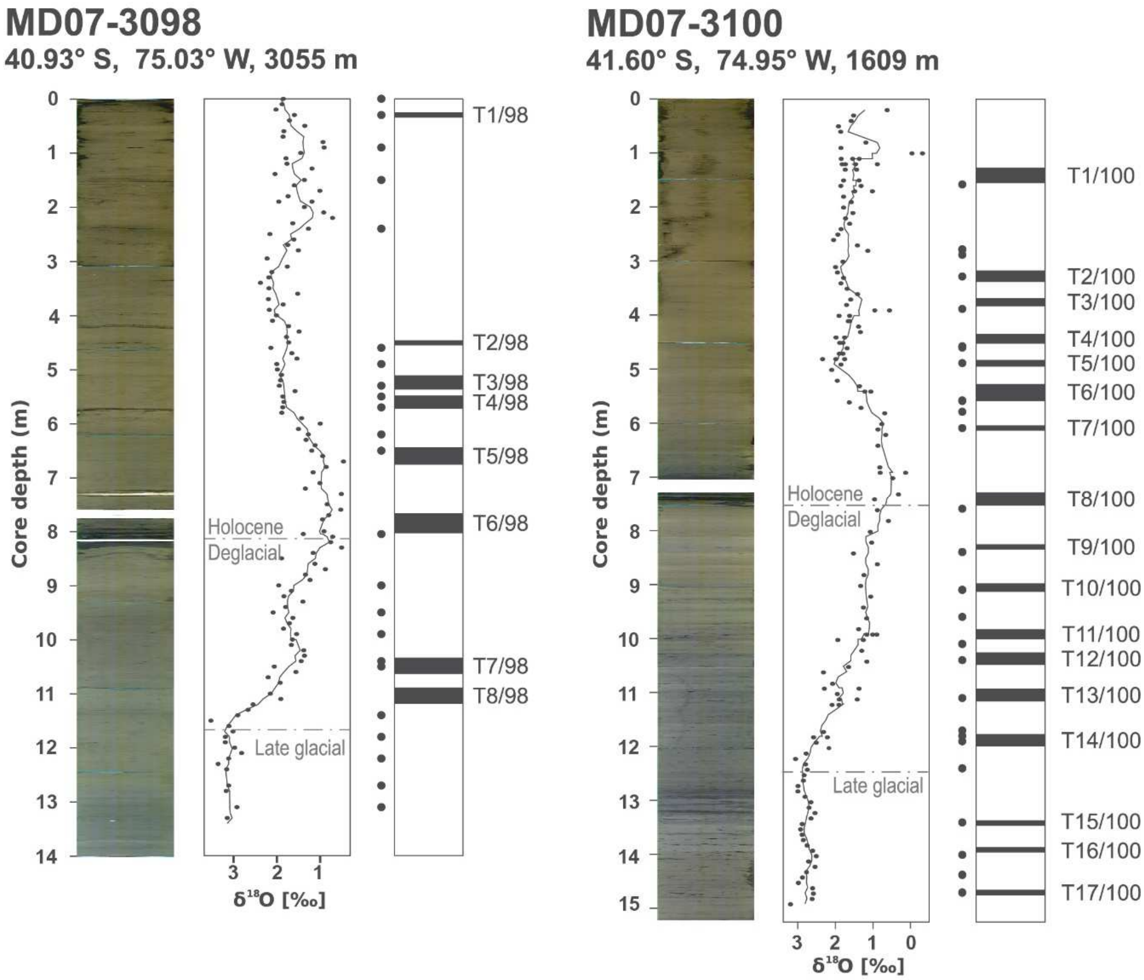

Figure 2. Stratigraphy from cores MD07-3098 and MD07-3100. Left: Composite photograph of each core, showing the position of the visible tephras as a dark layer at around 8 m (T6/98 in MD07-3098) and 7.5 m (T8/100 in MD07-3100). Middle: $\delta^{18}O$ from planktonic foraminifera G. bulloides; dots indicate measurements every 10 cm, the curve corresponds to the three point moving average. Also indicated are climate intervals inferred from the observed changes in $\delta^{18}O$. Right: Depths considered as potential cryptotephra layers (relative glass shard peaks) labeled T1/98 to T8/98 (MD07-3098) and T1/100 to T17/100 (MD07-3100), together with the position where planktonic foraminifera ^{14}C ages where obtained as dark grey dots. Details for $\delta^{18}O$ and ^{14}C measurements in core M07-3098 in Tables S1 and S5 and for core MD07-3100 in Haddam et al. (2018).

4.2 Cryptotephras

In core MD07-3100, sixteen depths where relative glass shard and micro–pumice peaks occurred were recognized as cyryptotephra layers labeled T1/100 to T17/100, in addition to T8/100 (Figure 2, Table 1). From the stable isotope stratigraphy, cryptotephra T1/100 through T7/100 occur during the Holocene, T8/100 in the Holocene/Deglaciation transition, T9/100 to T14/100 during the Deglaciation and T15/100, T16/100 and T17/100 during the late glacial.

In core M07-3098, seven depths where relative glass shard and micro–pumice peaks occur were identified as cryptotephra layers labeled T1/98 to T8/98, in addition to the visible tephra layer T6/8 (Figure 2, Table 1). T1/98 through T5/98 occur in the Holocene portion of the core, T6/98 in the Holocene/Deglaciation transition and T7/98 and T8/98 during the Deglaciation.

4.3 Geochemistry of the marine ash layers

All analyzed samples display major element composition belonging to the calc–alkaline series and most can be classified as medium–K to high–K, with rare glass shards of low-K affinity (Figure 3, 4, 5, Table S2, 3). Major elements in all samples follow a trend, either bimodal or continuous, ranging from basaltic andesite (minimum value of 49.8 wt.% SiO_2 in cryptotephra T8/100) to rhyodacite or rhyolite (maximum 77.8 wt.% SiO_2 in cryptotephra T9/100).

Three groups can be defined based on the relative amount of K_2O versus SiO_2:

- Group 1 (Figure 3, S5): samples with relatively high–K contents (0.7–3.9 wt.% K_2O), with basaltic andesitic (52–56 wt.% SiO_2), andesitic (56–63 wt.% SiO_2) and dacitic composition (63–70 wt.% SiO_2) plot along the boundary between medium and high-K fields (Peccerillo and Taylor, 1976) and points with rhyolitic composition in the high-K field (>70 wt.% SiO_2). The two visible tephras T6/98 and T8/100 and eleven cryptotephras among the twenty three analyzed, fall in this group, notably T1/100 through T7/100, T12/100, T14/100, T15/100 and T17/100;

Group 2 (Figure 4, S6): samples with relatively lower K contents than Group 1 (0.4–4.21 wt.% SiO_2). Basaltic andesitic and andesitic compositions plot in the medium–K field and sample points with dacitic and rhyolitic compositions at the boundary between medium–K and high–K. Eleven cryptotephras belong to this group: T1/98 through T5/98, T7/98, T9/100, T10/100, T11/100, T13/100, T16/100;

- Group 3 (Figure 5, S7): restricted to cryptotephra T8/98, which has consistently lower K contents (0.7–1.3 wt.% K_2O; with the exception of one outlier with high–K around 4.2 wt.% K_2O), plotting near the low/medium–K field boundary, especially at dacitic and rhyolitic composition.

Additionally, nine cryptotephras from core MD07-3100 were analyzed for trace elements: T1/100, T2/100, T4/100, T5/100, T6/100, T7/100, T9/100, T12/100, T14/100 and T15/100 together with tephra T8/100. Overall these samples are relatively enriched in the most incompatible elements (Rb, Ba, Th, U), have lower HFSE (negative anomaly of Nb, Ta) and lower REE and Sr contents and display a positive anomaly in Pb. Three different behaviors are observed when analyzing the La/Yb versus Zr/Nb ratios of the samples (Figure 3b, 4b): cryptotephra layers T2/100, T4/100, T5/100, T6/100, T7/100, T8/100, T12/100, T14/100 and T15/100 form a cluster with La/Yb values between ~4–7 and Zr/Nb between ~17–31; T1/100 has relatively higher La/Yb values between ~8–12 and Zr/Nb values between ~20–25; and T9/100 displays more dispersed values, with La/Yb between ~5–11 and Zr/Nb between ~18–30.

Cryptotephra	Core	Depth range (cm)	Calendar age median (years BP)	1σ range	2σ range	Group	Source	Potential correlative
T1/98	MD07-3098	25–35	294	445–132	747–62	Group 2		YA2?
T2/98	MD07-3098	445–455	6233	6410–5999	7053–5856	Group 1		
T3/98	MD07-3098	505–535	7633	7853–7320	8019–7027	Group 2		PCC2?
T4/98	MD07-3098	545–570	7928	8138–7738	8380–7639	Group 2		
T5/98	MD07-3098	645–675	9356	9581–9124	9916–8939	Group 2		PCC1?
T6/98	MD07-3098	764–801	10512	10702–10296	11265–10050	Group 1	Michinmahuida	Lepué
T7/98	MD07-3098	1030–1060	13965	14387–13681	14919–13546	Group 2		
T8/98	MD07-3098	1090–1120	15472	15778–15163	15991–14596	Group 3		
T1/100	MD07-3100	130–160	1557	1410–1720	1315–1855	Group 1	Hudson	HW7
T2/100	MD07-3100	320–340	3635	3895–3382	4118–3141	Group 1	Michinmahuida	LTT-10?
T3/100	MD07-3100	370–385	4117	4342–3939	4424–3745	Group 1		
T4/100	MD07-3100	440–460	6170	6694–5716	6992–5122	Group 1	Michinmahuida	LTT14? LTT-15? MIC1?
T5/100	MD07-3100	485–495	7044	7214–6838	7520–6686	Group 1	Michinmahuida	LTT15? MIC1?
T6/100	MD07-3100	530–560	8514	8636–8364	8812–8228	Group 1	Michinmahuida	LTT20?
T7/100	MD07-3100	605–615	9603	9703–9478	9892–9318	Group 1	Michinmahuida	
T8/100	MD07-3100	728–755	10616	10706–10440	10938–10348	Group 1	Michinmahuida	Lepué
T9/100	MD07-3100	825–835	12163	12464–11941	12604–11760	Group 2		
T10/100	MD07-3100	895–915	12839	12966–12671	13151–12575	Group 2		
T11/100	MD07-3100	980–1005	13812	13906–13672	14047–13596	Group 2		
T12/100	MD07-3100	1025–1050	14154	14296–13950	14533–13808	Group 1	Michinmahuida	
T13/100	MD07-3100	1125–1145	15253	15493–15048	15701.5–14777	Group 2		
T14/100	MD07-3100	1170–1190	15930	16063–15775	16228–15649	Group 1	Michinmahuida	
T15/100	MD07-3100	1340 cm	18226	18422–18030	18595–17870	Group 1	Michinmahuida	
T16/100	MD07-3100	1390 cm	19386	19709–19193	19900–18758	Group 2		
T17/100	MD07-3100	1470 cm	20448	20638–20266	20818–20080	Group 1		

Table 1. Summary of identified tephras and cryptotephras in cores MD07-3098 and MD07-3100.

5. Correlations

For the identification of the potential source of the tephras and cryptotephras, we compared the geochemistry of the glass shards here analyzed with the geochemistry of both explosive and effusive products that were analyzed by both micro analytical and bulk geochemical methods from volcanic centers between Llaima and Hudson. The latter is achieved taking into account that for some of the volcanic centers in this area no micro analytical data were found in the literature (e.g. Yanteles and Corcovado by Naranjo and Stern (2004)) and that, especially for older eruptions, only effusive products were analyzed (e.g. Puyehue-Cordón Caulle by (Singer et al., 2008)). Additionally, previous work in the region has previously shown that a similar geochemical trend is followed by effusive and explosive products from the Hudson volcano (Carel et al., 2011), which is also observed in the literature here considered (Figure S8, S9). Most of this literature corresponds to major element compositions, from which it can be observed that the major element signature of many volcanoes overlap (Figure S10). Thus major element compositions cannot be used alone to pinpoint the volcanic source of the cryptotephras. Nevertheless, the potential volcanic sources can still be narrowed down based on their K_2O versus SiO_2 contents. With this in mind, in the following section, we organize the discussion regarding the potential source of the tephras and cryptotephras according to the three groups previously defined based on the relative amount of K_2O versus SiO_2 together with some key trace element ratios of the analyzed samples, when available (Figure 3, 4, 5). The potential eruptive event is further constrained based on the stratigraphy and estimated age of the tephras and cryptotephras.

5.1 Group 1

The thirteen tephras and cryptotephras belonging to Group 1, with relatively higher K (0.7–3.9 wt.% K_2O), especially at silica levels higher than ~68 wt.% SiO_2 (Figure 3a, S4), display a geochemical trend similar to volcanoes Michinmahuida (Alloway et al., 2017a; Amigo et al., 2013; Naranjo and Stern, 2004), Hudson (Carel et al., 2011; Del Carlo et al., 2018; Haberle and Lumley, 1998; Kratzmann et al., 2008; López-Escobar et al., 1993; Naranjo et al., 1993; Naranjo and Stern, 1998; Smith et al., 2019; Stern, 2008; Weller et al., 2015, 2014), Quetrupillán (Brahm et al., 2018; Fontijn et al., 2016; Hickey-Vargas et al., 1989; Rawson et al., 2016; Simmons et al., 2020) and Yate (López-Escobar et al., 1993; Mella, 2008; Watt et al., 2011b). These volcanic centers can be further discriminated by means of their trace element geochemistry, in particular, their Zr/Nb versus La/Yb ratios (Figure 3b). From the thirteen tephras and cryptotephras in this group, one tephra and nine cryptotephras have been analyzed for trace elements: T1/100, T2/100, T4/ 100, T5/100, T6/100, T7/100, T8/100, T12/100, T14/100 and T15/100. When comparing their Zr/Nb versus La/Yb ratios, with the available information from Michinmahuida, Hudson, Quetrupillán and Yate, the tephra (T8/100) and eight of the nine cryptotephra layers (T2/100, T4/100, T5/100, T6/100, T7/100, T12/100, T14/100 and T15/100) display compositions similar to Michinmahuida and one cryptotephra (T1/100) displays compositions similar to Hudson. Similar behaviors are observed when looking at other trace elements (Figure S11), such as Zr versus Y, La versus Tm and Th versus Nb, although the differences among the different volcanic centers are not as clear as in the case of La/Yb versus Zr/Nb.

In addition, one potential correlation among the marine sediment cores can be established

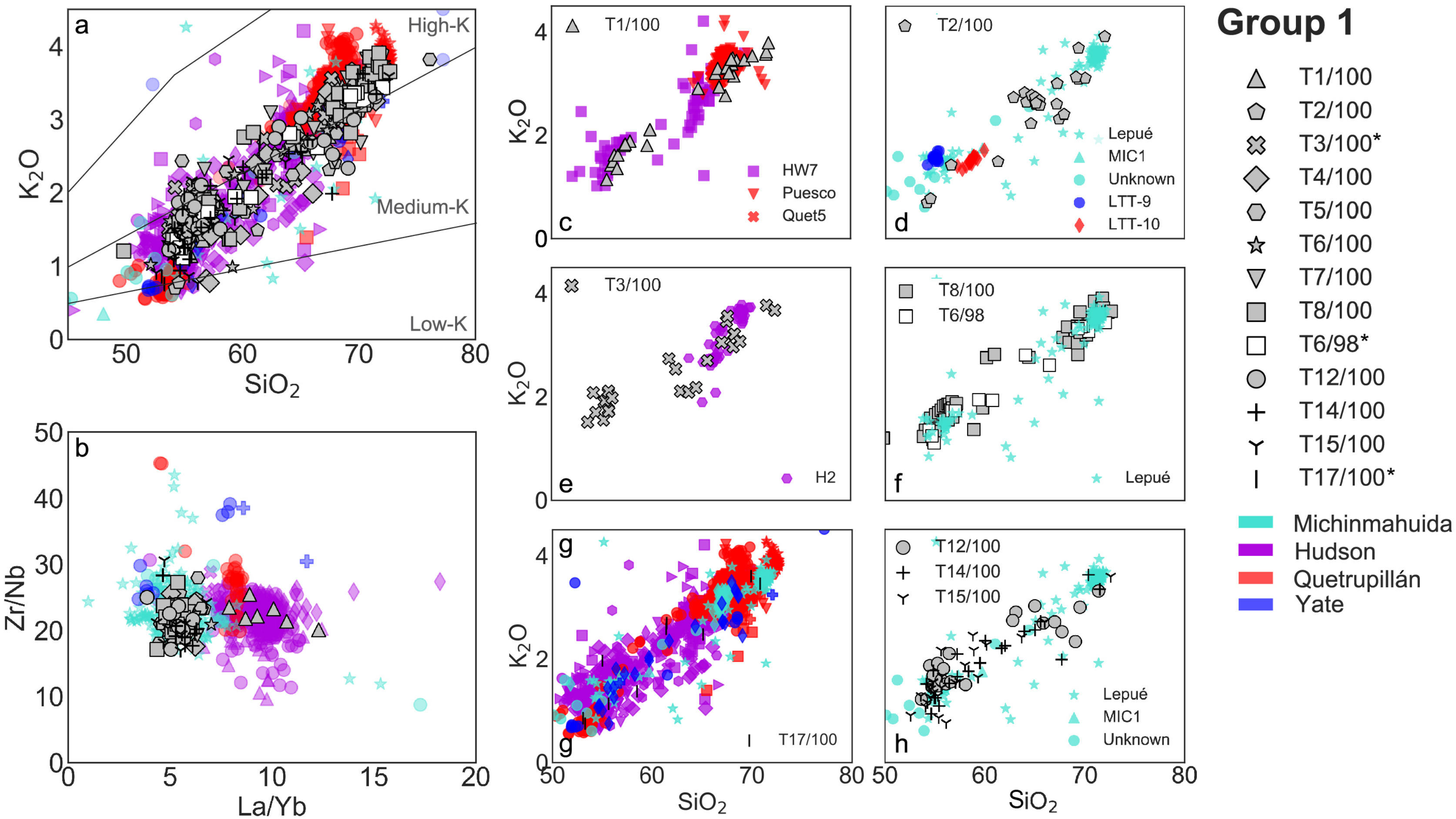

Figure 3. Individual glass shard composition from the cryptotephra layers here studied corresponding to Group 1 (legend to the right). The latter are compared with available analyses of post–glacial deposits from volcanic centers displaying a similar behavior (color legend to the right): Michinmahuida (Alloway et al., 2017a; Amigo et al., 2013; López-Escobar et al., 1993; Naranjo and Stern, 2004), Hudson (Carel et al., 2011; Del Carlo et al., 2018; Haberle and Lumley, 1998; Kilian et al., 2003; Kratzmann et al., 2008; López-Escobar et al., 1993; Naranjo et al., 1993; Naranjo and Stern, 1998; Smith et al., 2019; Stern, 2008; Weller et al., 2014, 2015), Quetrupillán (Brahm et al., 2018; Fontijn et al., 2016; Hickey-Vargas et al., 1989; Rawson et al., 2016) and Yate (López-Escobar et al., 1993; Mella, 2008; Watt et al., 2011b). "Unknown" corresponds to products not assigned to any particular eruption. a: All cryptotephras in Group 1 are plotted, lines separating areas with low–K, medium–K and high–K according to Peccerillo and Taylor (1976) are shown. b: Only tephra for which trace elements were analyzed are shown (cryptotephra without an asterisk in the legend to the right). c, d, e, f, g, h: Comparison of specific cryptotephra where a potential correlative could be identified on land with available geochemical analyses. c: HW7 (Haberle and Lumley, 1998), Puesco and Quet5 (Fontijn et al., 2016). d: LTT-9 and LTT-10 (Moreno et al., 2014) together with available post–glacial data from Michinmahuida (Lepué, MIC1 and Unknown). e: H2 (Haberle and Lumley, 1998; Naranjo and Stern, 1998; Smith et al., 2019; Weller et al., 2015). f: Lepué (Alloway et al., 2017a; Amigo et al., 2013). g: same as a. h: available post–glacial data from Michinmahuida (Lepué, MIC1 and Unknown). Major element data correspond to normalized volatile–free compositions.

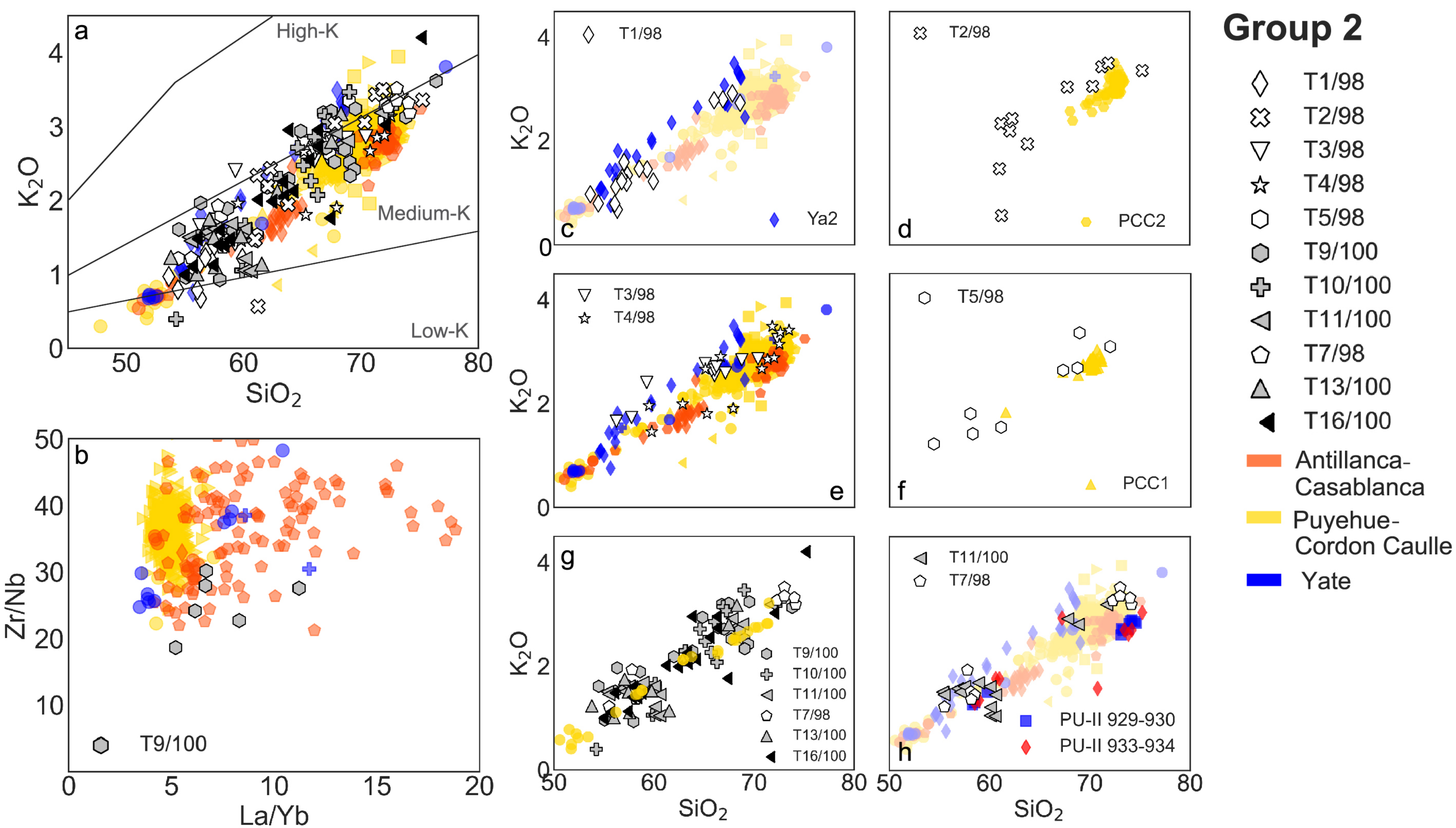

Figure 4. Individual glass shard composition from the cryptotephra layers here studied corresponding to Group 2 (legend to the right). The latter are compared with available analyses of post–glacial deposits from volcanic centers (color legend to the right) displaying a similar behavior: Puyehue-Cordón Caulle (Alloway et al., 2015; Bertrand et al., 2008; Fontijn et al., 2016; Gerlach et al., 1988; Lara et al., 2006; Naranjo et al., 2017; Rawson et al., 2016; Singer et al., 2008), Antillanca-Casablanca (Fontijn et al., 2016; Geoffroy et al., 2018; Jacques et al., 2014; Naranjo et al., 2017; Rawson et al., 2016; Villarosa et al., 2006) and Yate (López-Escobar et al., 1993; Mella, 2008; Watt et al., 2011b). a: All cryptotephras in Group 2 are plotted, lines separating areas with low–K, medium–K and high–K according to Peccerillo and Taylor (1976) are shown. b: Trace element comparison between T9/100 and available information from volcanic centers in Group 2. c, d, e, f, g, h: Comparison of specific cryptotephras were a potential correlative could be identified on land with available geochemical analyses. c: Glass shards analyses from Ya2 (Watt et al., 2011b) are highlighted. d and f: Comparison with glass shard analyses of PCC2 and PPC1 by Fontijn et al. (2016) and bulk tephra by Singer et al. (2008), Rawson et al. (2016) and Naranjo et al. (2017). g: Comparison of deglacial and late glacial cryptotephras with deglacial products from Puyehue-Cordón Caulle, whole–rock analyses by Singer et al. (2008) dated by $^{40}Ar/^{39}Ar$ in 13.2 ± 2 and 18.7 ± 2.1 cal ka BP; post–glacial whole–rock analyses by Gerlach et al. (1988). h: comparison of T7/98 and T11/100 with tephra PU-II 929-930 and 933-934 cm (Bertrand et al., 2008). Major elements correspond to normalized volatile–free compositions.

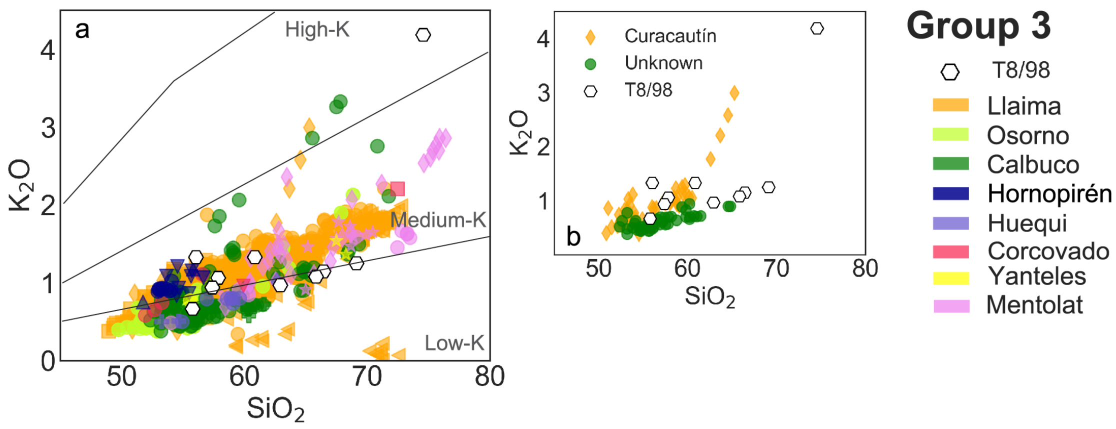

Figure 5. Individual glass shard composition from the cryptotephra here studied corresponding to Group 3 (T8/98, legend to the right). T8/98 is compared with post–glacial analyses from volcanic centers (color legend to the right) displaying a similar behavior: Llaima (Bouvet de Maisonneuve et al., 2012; Naranjo and Moreno, 1991, 2005; Rawson et al., 2016; Reubi et al., 2011; Schindlbeck et al., 2014; Lohmar, 2008), Osorno (Bertrand et al., 2008; Jacques et al., 2014; López-Escobar et al., 1993; López-Escobar et al., 1992; Moreno et al., 2010; Tagiri et al., 1993), Calbuco (López-Escobar et al., 1995, 1992; Morgado et al., 2019; Watt et al., 2011b; Sellés and Moreno, 2011), Huequi, Hornopirén (Watt et al., 2011a, b), Mentolat (López-Escobar et al., 1993; Naranjo and Stern, 2004; Stern et al., 2015; Weller et al., 2017, 2015) Yanteles and Corcovado (López-Escobar et al., 1993; Naranjo and Stern, 2004). b: comparison with Curacautín tephra products: glass shards (Fontijn et al., 2016), matrix glass (Lohmar, 2008) and bulk tephra (Naranjo and Moreno, 2005; Lohmar, 2008; Schindlbeck et al., 2014) and eruptive products not assigned to any particular eruption from Calbuco, marked as "Unknown" (Sellés and Moreno, 2011). Major elements correspond to normalized volatile–free compositions.

for tephras T6/98 and T8/100 since they display similar major element geochemistry and occur in a similar stratigraphic position (Figure 2, 3f, 6).

In the following section we discuss the potential correlative of each cryptotephra based on its stratigraphic position, estimated calendar age and available geochemical information on land from the potential sources. Because many of the cryptotephras display a Michinmahuida signature, we discuss them together.

5.1.1. T1/100

The stratigraphic position of this cryptotephra corresponds to the Late Holocene, with an estimated mean calendar age at its base of ~1.6 (1σ: 1.7–1.4) cal ka BP (Table 1). Around this time, two of the volcanic centers associated with Group 1: Hudson and Quetrupillán, had eruptions recorded in the literature (Figure 6): HW7 from Hudson (~1.5 cal ka BP; 1σ:

1.7–1.4; Haberle and Lumley, 1998), Quet5 (~1.7 cal ka BP; 1σ: 1.8–1.6) and Puesco (~1.9 cal ka BP; 1σ: 2–1.8; Fontijn et al., 2016) from Quetrupillán. Individual glass shard major element geochemistry has been obtained for all of these eruptions and therefore we can compare their geochemical fingerprints with those of the marine cryptotephras (Figure 3c). From these, T1/100 displays values closer to HW7 (Carel et al., 2011; Haberle and Lumley, 1998), both of which follow a bimodal trend. In contrast Quet5 and Puesco only display more evolved products, between 65–68 wt.% SiO_2, thus the less evolved part of the trend, observed in T1/100, is absent. Major and trace element data thus support the Hudson volcano as the source of the T1/100 cryptotephra (Figure 3a, b, c, S7). We propose T1/100 as a distant correlative of the HW7 eruption of the Hudson volcano. The latter is consistent with prior information indicating a northwest dispersion of some Hudson volcano products (Figure 6) such as eruptions HW2, HW3, HW6, HW1 and HW7, found in lake cores in Taitao peninsula and Chonos archipelago (Haberle and Lumley, 1998) as well as in marine sediment core MD07-3088 (Carel et al., 2011).

5.1.2 T3/100

Cryptotephra T3/100 occurs in the Late Holocene at an estimated calendar age of ~4.1 (1σ: 4.3–3.9) cal ka BP. During this time period, from the volcanoes in Group 1, only Hudson has a recorded eruption (Figure 6): H2 at ~4 cal ka BP (Naranjo and Stern, 1998). From the comparison of the major element geochemistry, it is plausible that T3/100 corresponds to the eruption H2 (Figure 3e), however H2 corresponds to fairly evolved products ranging from 64–70 wt.% SiO_2 whereas T3/100 also presents a less evolved cluster between 54–56% SiO_2 not present in H2, as documented in the literature. As mentioned before, the major element geochemistry of T3/100 is also consistent with Yate, Michinmahuida and Quetrupillán (Figure S8). The source of this cryptotephra could be further constrained by trace element analyses and future research around these volcanoes which might reveal other potential correlatives.

5.1.3 T17/100

T17/100, occurs in the Late glacial at an estimated age of ~20.5 (1σ: 20.6–20.3) cal ka BP. From the major elements alone is not possible to further narrow down among the volcanic centers in Group 1 as the possible source (Figure 3g, S9). Additionally, little evidence for tephra deposits at this time exists on land because of the predominant presence of the PIS in the area until ~18 cal ka BP (Davies et al., 2020). From the volcanoes in Group 1, so far only volcanic products from Yate have been dated so far, by $^{40}Ar/^{39}Ar$ in 22 ± 7 cal ka BP (Mella, 2008), indicating volcanic activity during this time. No evidence for Michinmahuida, Hudson or Quetrupillán at this time exists so far, however because of the position of Quetrupillán north of the sediment core, which is opposite to the predominant winds in the area, it is less likely that T17/100 was emitted from this volcano.

5.1.4 Cryptotephras with Michinmahuida signature

We now discuss the potential correlations of the tephra and cryptotephra layers which have geochemical compositions similar to the Michinmahuida volcano, as discussed above (T2/100, T4/100, T5/100, T6/100, T7/100, T8/100, T6/98, T12/100, T14/100 and T15/100).

5.1.4.1 T2/100

The younger cryptotephra with a geochemistry similar to Michinmahuida volcano is T2/100 (Figure 3a, b, d) with an estimated age of ~3.6 cal ka BP (1σ: 3.9–3.4). In the literature, evidence for eruptive activity of this volcano at that time has been found in a lacustrine core

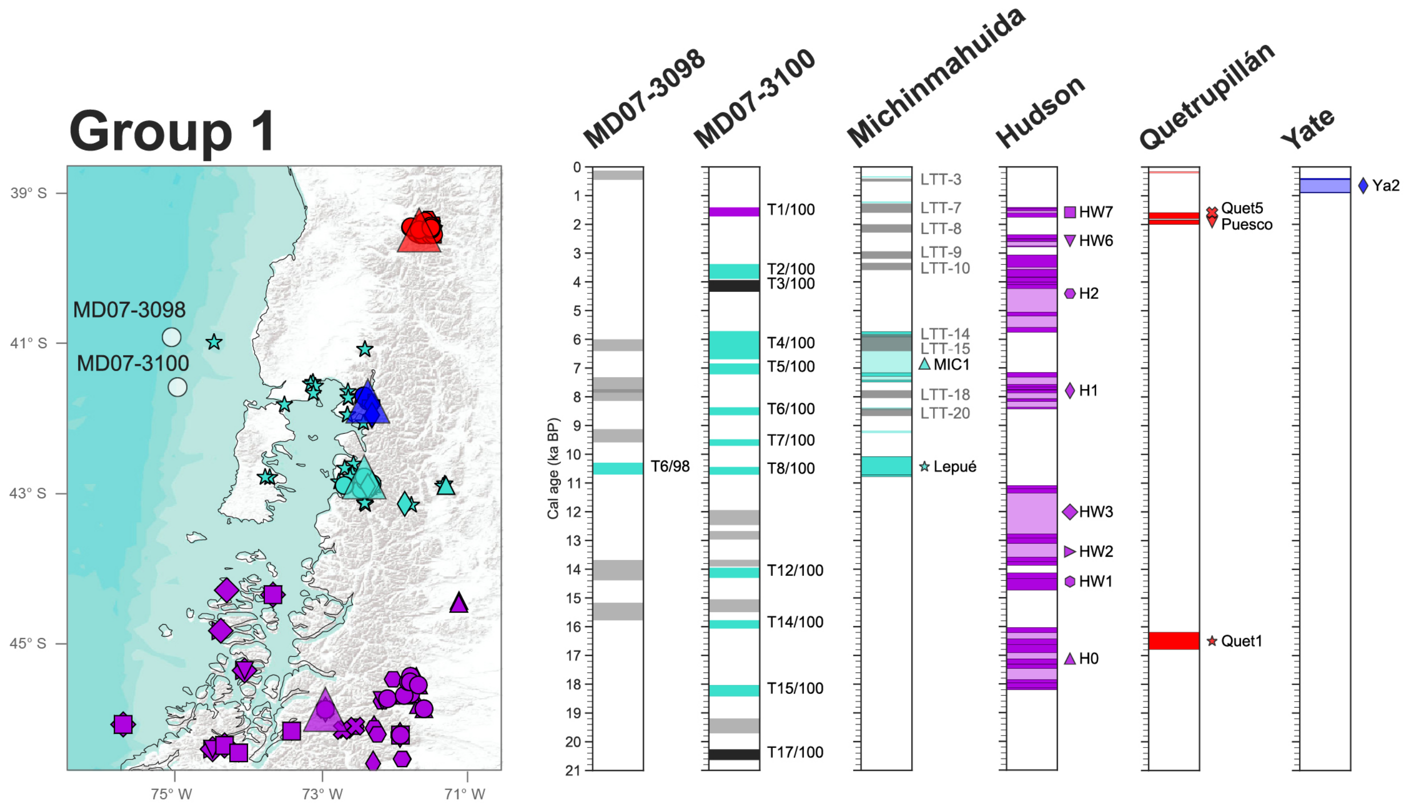

Figure 6. Chronology for cores MD07-3098 and MD07-3100 highlighting the cryptotephras associated to Group 1, as described in the text, compared with the chronologies of explosive products from each volcanic center displaying a similar geochemical behavior (Figure 3). Only known events dated by ^{14}C are plotted. To the left: position of the marine sediment cores here studied together with the position of each volcanic center associated to Group 1 indicated as a triangle, from north to south: Quetrupillán, Yate, Michinmahuida and Hudson. Also shown are the position of tephrochronological samples which have been analyzed for geochemistry and/or dated as smaller size symbols. Each symbol corresponds to a different eruptive event indicated in the respective volcanic center chronology (to the right). Pyroclastic deposits which have been dated but no correlation has been yet established are plotted in the chronology as colored rectangles of the corresponding volcanic center color, but they are unlabeled (no symbol or name is indicated to their right) and their position is indicated as a dot of the corresponding volcanic center color in the map. These samples are labeled "Unknown" in Table S6. Details on the chronologies of each volcanic center in Table S6.

~24 km southwest of Michinmahuida at Lago Teo (~42.9° S, ~72.7° W; Moreno et al., 2014) and in the Mallines section ~13 km southeast of it (~42.9° S, ~72.3° W; Amigo et al., 2013). In the Mallines section, Amigo et al. (2013) report a scoria deposit identified in the upper part of the section (*3rd scoria*), bracketed between ~5 and 1.3 cal ka BP, which they attribute to the Michinmahuida volcano. For this deposit, major and trace elements were analyzed in the bulk tephra, however the sample has been reported as altered (Amigo et al., 2013) so further robust correlation is not possible. At Lago Teo, on the other hand, four tephras with a Michinmahuida–like major element geochemistry have been identified between ~5–1.3 cal ka BP by Moreno et al. (2014). From these, the more likely correlatives to T2/100 correspond to LTT-9 and LTT-10 (Figure 6), which have estimated calendar ages of ~3 (1σ: 3.2–2.9) and ~3.5 (1σ: 3.6–3.3) ka BP. However, it is not possible to establish a robust correlation because the majority of the analyzed glass shards in T2/100 correspond to the more evolved part of the trend with dacitic and rhyolitic compositions, which are not present in LTT-9 and LTT-10.

5.1.4.2 T4/100 and T5/100

During the Middle Holocene, two cryptotephras with a Michinmahuida signature occur in the marine sediment cores: T4/100 and T5/100. T4/100 has a calibrated age of ~6.2 (1σ: 6.7–5.7) cal ka BP, whereas T5/100 has an age of ~7 (1σ: 7.2–6.8) cal ka BP.

At Lago Teo, two tephras occur in the Middle Holocene (LTT-14 and LTT-15), which have respectively estimated calendar ages of ~6.1 (1σ: 6.3–5.8) and ~6.2 (1σ: 6.4–6) cal ka BP (Moreno et al., 2014), and have been suggested to follow a geochemical trend similar to Michinmahuida. From these, LTT-14 displays values with lower K (Figure 7a) than commonly reported for Michinmahuida, meanwhile the composition of LTT-15 is closer to Michinmahuida and to the less evolved part of the trend in both T4/100 and T5/100 (Figure 7a). The estimated calendar ages of LTT-15 and LTT-14 overlap (Figure 6) and they are both within error synchronous to T4/100, hence it is not possible to further correlate these deposits.

Additionally, both T4/100 and T5/100 could potentially be correlated to the MIC1 tephra from Michinmahuida volcano (Amigo et al., 2013; Naranjo and Stern, 2004). The MIC1 tephra was first identified as an andesitic pumice deposit ~90 km east of Michinmahuida volcano by Naranjo and Stern (2004). They obtained two ^{14}C ages from peat bracketing the MIC1 deposit, which indicate an age equal to or younger than ~7.2 and older than ~5.8 cal ka BP (Figure 6, Table S6). A correlative of this tephra was later identified by Amigo et al. (2013) in the Mallines section, who dated the underlying paleosol at ~7.5 cal ka BP. However, a younger age was obtained in the same paleosol a few centimeter below, indicating this age altered by Amigo et al. (2013), thus a robust correlation based on geochemistry cannot be done. However, from the sole available analysis, major elements display similar values to T4/100 and T5/100 (Figure 7a). Additional evidence for eruptive activity of Michinmahuida during this time is also provided by Alloway et al. (2017b), who describe the occurrence of a tephra layer in various sections (Pumalín-3, -4, -7, -2) in the area nearby Michinmahuida volcano occurring directly under Pumalín/Cha2 tephra, coincident with the position of MIC1 in the Mallines section. One trace element analysis in Pumalín-2 section (Pum 2-11) is provided by Alloway et al. (2017a) in bulk tephra, which displays a Michinmahuida–like geochemistry (Figure 7b).

From a chronological point of view, it is possible that T4/100 is correlated to LTT-15 (and/or

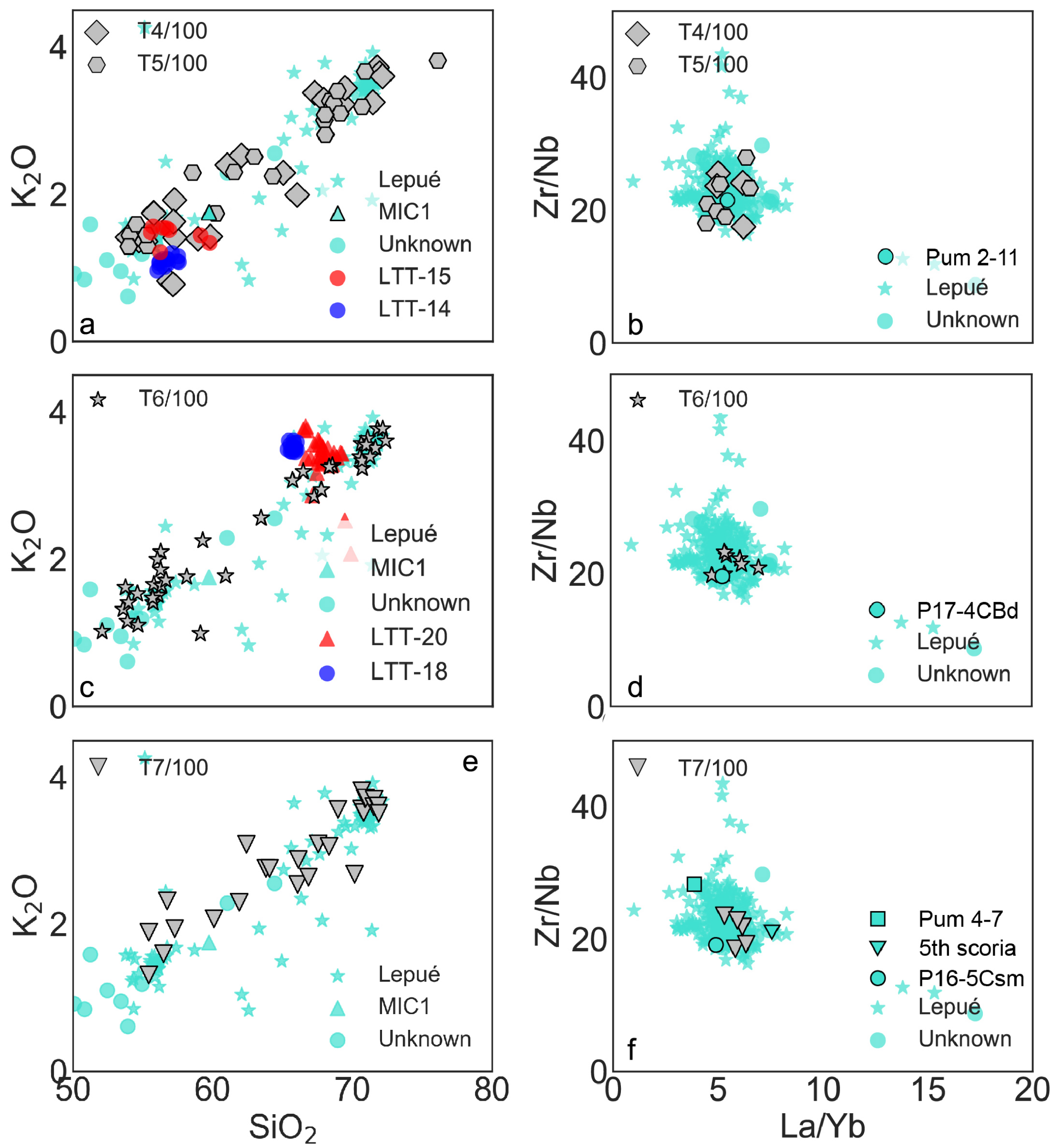

Figure 7. Comparison of specific crytotephras belonging to Group 1 displaying a Michinmahuida signature with potential correlatives on land. In all cases all the available information from Michinmahuida is plotted as cyan symbols in the background (Alloway et al., 2017a; Amigo et al., 2013; López-Escobar et al., 1993; Naranjo and Stern, 2004) and specific correlatives are indicated in the legend. LTT-14, LTT-15, LTT-18 and LTT-20 (Moreno et al., 2014), MIC1 (Amigo et al., 2013; Naranjo and Stern, 2004), Pum 2-11 and Pum 4-7 (Alloway et al., 2017b), P17-4CBd and P16-5Csm (Casati et al., 2019), 5th scoria (Amigo et al., 2013), Lepué (Alloway et al., 2017a; Amigo et al., 2013), Unknown correspond to products not assigned to any particular eruption (Amigo et al., 2013; López-Escobar et al., 1993). Major elements correspond to normalized volatile–free compositions.

estimate might not be accurate. Unfortunately, only three geochemical data points identified as MIC1 are provided in the literature, all in bulk samples, two of which are thought to be

LTT-14) and that T5/100 is correlated to MIC1. Additionally, because of the large uncertainty associated with the age of MIC1, it is also possible that LTT-15 and T4/100 are correlatives of MIC1 (Figure 6) and that no correlative of LTT-15 has been identified.

5.1.4.3 T6/100

T6/100 occurs in the Early Holocene and has an estimated calendar age of ~8.5 cal ka BP (1σ: 8.6–8.3). Evidence of Michinmahuida activity around this time is again found in Lago Teo and in one section nearby the village of Chaitén (Casati et al., 2019). Casati et al. (2019) identified a Michinmahuida–sourced deposit dated in ~8.4 cal ka BP (1σ: 8.4–8.3) for which one geochemical analysis is available displaying La/Yb versus Zr/Nb ratios coincident with T6/100 (Sample P17-4CBd, Figure 7d), thus we propose this deposit is a likely correlative of T6/100. In Lago Teo, two tephras identified as Michinmahuida occur during this period: LTT-18 and LTT-20 with calendar age estimates for tephra LTT-18 of ~ 7.9 cal ka BP (2σ: 8–7.8) and of ~8.5 cal ka BP (2σ: 8.6–8.4) for LTT-20. Thus, LTT-20 could correspond to T6/100. When comparing the major element geochemistry, LTT-20 represents a cluster around 68 wt.% SiO_2, whereas T6/100 is rather bimodal with a wider range of compositions, almost identical to Lepué tephra (Figure 7c). However, they might still correspond to the same tephra, and further information might reveal in the future a wider compositional range for the eruption that formed LTT-20.

5.1.4.4 T7/100

T7/100 is the oldest cryptotephra that occurs in the Early Holocene, which has an estimated age of ~9.6 cal ka BP (1σ: 9.7–9.5). Evidence on land for Michinmahuida activity around this time is presented by Casati et al. (2019), who dated a deposit attributed to Michinmahuida at ~9.2 cal ka BP (1σ: 9.3–9.2), very similar to the estimated calendar age for T7/100 (Figure 6). Amigo et al. (2013) identify one scoria deposit (*5th scoria* in the Mallines section) from Michinmahuida and bracket this event between ~7.6 and 10.3 cal ka BP. This deposit is positioned above Cha1 tephra, for which a calibrated age estimate ranging from ~9.5 to 10.5 cal ka BP has been proposed (Alloway et al., 2017b; Amigo et al., 2013; Fontijn et al., 2016; Naranjo and Stern, 2004; Watt et al., 2011b). A potential correlative of this deposit is also identified by Alloway et al. (2017b) in section Pumalín-4, which occurs above Cha1 as the *5th scoria* from the Mallines section and is proposed to have a geochemical composition corresponding to Michinmahuida. A comparison of the element measurement for Pumalín-4 (Pum 4-7), the deposit (P16-5Csm) identified by Casati et al. (2019) and the *5th scoria*, display La/Yb versus Zr/Nb values close to those know for Michinmahuida and to T7/100 (Figure 7f).

5.1.4.5 T6/98 and T8/100

T6/98 and T8/100 correspond to the only visible tephras in cores MD07-3098 and MD07-3100, respectively. Both tephras occur in the same stratigraphic position in each core at the Holocene-Deglaciation transition, and at synchronous calendar ages, within error, of ~10.6 (1σ: 10.7–10.4) for T8/100 and ~10.5 (1σ: 10.7–10.3) cal ka BP for T6/98 (Figure 6). Additionally, they both have a thickness of ~25–30 cm and similar major element geochemistry (Figure 3f), thus we propose that both tephras are correlatives. The major element compositions tend to be bimodal with two clusters at 54–57 and 68–73 wt.% SiO_2 and both major and trace elements are consistent with volcanic deposits attributed to Michinmahuida, in particular the Lepué tephra (Figure 3f).

So far, only one deposit from Michinmahuida volcano has been thoroughly described in the literature: the Amarillo Ignimbrite/Lepué Tephra. The Amarillo Ignimbrite was first described and dated by Amigo et al. (2013) in the vicinities of Michinmahuida volcano. However because of the lack of geochemical information they were not able to identify the fall deposit associated with the eruption. Later, Alloway et al. (2017a) identified and described the associated regional tephra and named it Lepué because of its occurrence in and around Lago Lepué on Chiloé island, northwest of the Michinmahuida volcano. This is a tephra with a bimodal composition with values ranging from ~54–72 wt.% SiO_2 (Figure 3f), with an estimated calendar age around 10.9 cal ka BP (Alloway et al., 2017a). The Lepué tephra has been identified in dozens of different sites, as far away as ~250 km northwest from the Michinmahuida volcano (Figure 6), with a predominantly northern and northwestern dispersion (Alloway et al., 2017a). In particular, it has been identified on the Chilean continental margin at ODP-202 site 1233, located ~20 km southeast of marine core MD07-3098 and 50 km northeast of core MD07-3100. At ODP-202 site 1233, the Lepué tephra is ~30 cm thick and its age is bracketed between ~10 and 12.3 cal ka BP (Alloway et al., 2017a). The latter is consistent with the visible tephra layers of ~25–30 cm thick found in cores MD07-3100 and MD07-3098. Furthermore, when comparing their trace and major element geochemistry, both tephras in the studied cores are consistent with the Lepué

Tephra products (Figure 3b, f). Thus we identify the only visible tephra in the cores as the regional marker Lepué tephra.

5.1.4.6 T12/100, T14/100, T15/100

Cryptotephras T12/100, T14/100 and T15/100 have estimated calendar ages of ~14.2 (1σ: 14.3–14), ~15.9 (1σ: 16.1–15.8) and ~18.2 (1σ: 18.4–18) cal ka BP. No tephra with a geochemistry similar to Michinmahuida has been thoroughly described during the Deglaciation and late glacial and more particularly, none older than Lepué tephra. The lack of Michinmahuida tephras could be related to the presence of the PIS in the area proximal to the volcano in the last glacial period. However, a recent study in the La Zeta sequence located in the Argentina sector of the Andean complex has allowed to recover some tephras whose origin has been tentatively attributed to the Michinmahuida, however no geochemistry is available for further comparison (Alloway et al., 2017b). In particular, the JT1 tephra dated at ~18 cal ka BP (1σ: 18.2–17.8) has an age similar to that of the T15/100 event (~18.2 cal ka BP). Additionally, Alloway et al. (2017b) identify two other deposits, JT4 and JT5 with age estimates of 17.8 (1σ: 17.9–17.6) and 17.5 (1σ: 17.6–17.3) cal ka BP. These ages are not coincident with any of the marine cryptotephras here identified, however they represent an evidence of volcanic activity of the Michinmahuida volcano during deglacial period.

As a summary, it was possible to robustly identify two eruptions from the Group 1 tephras and cryptotephras: the Lepué tephra from Michinmahuida (T6/98 and T8/100), occurring at ~10.9 cal ka BP; and the HW7 tephra from the Hudson volcano (T1/100), occurring at ~1.5 cal ka BP. Both of which have been shown to record a northwestern dispersion (Figure 6;

Alloway et al., 2017a; Carel et al., 2011;Haberle and Lumley, 1998). Additionally, eight cryptotephras layers where identified as Michinmahuida–sourced (T2/100, T4/100, T5/100, T6/100, T7/100, T12/100, T14/100 and T15/100). These results are consistent with previous research around Michinmahuida volcano which had suggested recurrent volcanic activity during the Holocene (Amigo et al., 2013; Moreno et al., 2014). However, it is still hard to provide robust correlations among deposits, which in part is due to the paucity and accuracy of age/stratigraphic constraints, major and/or trace elements geochemistry. Additionally, the apparent high recurrence of Michinmahuida volcano can also be a source of uncertainty in the correlation since age estimates might not be precise enough to distinguish among eruptions, as in the case of LTT-14 and LTT-15 (Figure 6). Here we combine age/stratigraphic constraints, major and/or trace elements geochemistry to provide robust correlatives for Michinmahuida–sourced tephras, in the ocean. The occurrence of tephras older than T8/100 (T2/100, T14/100 and T15/100, Figure 6) is particularly interesting because it provides robust new evidence for recurrent activity of the Michinmahuida volcano since the late glacial period. This new information might be missing on land because of the highly vegetated area, less research around Michinmahuida because of its inactivity in historical times, or because of glacial erosion associated to the presence of the PIS. In many sites the Lepué tephra was found lying above glacial deposits (Alloway et al., 2017a), however in some other sites additional tephra deposits have been found between Lepué and glacial till and more so, organic matter directly above glacial deposits has been dated as old as ~17 cal ka BP. In fact, estimates of the PIS extent since the Last Glacial Maximum indicate that a rapid retreat would have begun in this area around 18 cal ka BP and that by 15 cal ka BP the ice was confined to the vicinities of the volcanoes (Davies et al., 2020), allowing for the deposition of deglacial tephras on land. Thus, it might be possible to find on land correlatives for the Michinmahuida cryptotephras discussed here. In particular, deposits tentatively associated with Michinmahuida have already been mentioned in the literature (Alloway et al., 2017a), which might be correlated if geochemical information becomes available.

5.2 Group 2

Cryptotephra layers T1/98, T2/98, T3/98, T4/98, T5/98, T9/100, T10/100, T11/100, T7/98, T13/100, T16/100 display a major element trend similar to that of volcanic centers Antillanca-Casablanca (Fontijn et al., 2016; Naranjo et al., 2017; Geoffroy et al., 2018; Villarosa et al., 2006), Puyehue-Cordón Caulle (Figure 4, S5; Alloway et al., 2015; Bertrand et al., 2014; Fontijn et al., 2016; Gerlach et al., 1988; Lara et al., 2006; Naranjo et al., 2017; Singer et al., 2008; Villarosa et al., 2006) and Yate (López-Escobar et al., 1993; Mella, 2008; Watt et al., 2011b). T1/98 occurred in the Late Holocene; T2/98, T3/98, and T4/98 occurred in the Middle Holocene; T5/98 in the Early Holocene; T9/100, T10/100, T11/100, T7/98 and T13/100 during the Deglaciation; and T16/100 during the late glacial (Figure 2, 8).

Three eruptions sourced from Antillanca-Casablanca have been recognized so far in the literature: Nahuel Huapi (Fontijn et al., 2016; Naranjo et al., 2017), Rayhuen (Fontijn et al., 2016) and Playas Blanca-Negra (Fontijn et al., 2016; Geoffroy et al., 2018; Naranjo et al., 2017; Villarosa et al., 2006). All of them have been dated and occurred between ~1.3–3.5 cal ka BP (Fontijn et al., 2016; Naranjo et al., 2017; Villarosa et al., 2006) and cannot be correlated with any of the cryptotephras studied here (Figure 8). In the case of Puyehue-Cordón Caulle, five Holocene tephras deposits are described in the literature: Mil Hojas, North Cordón Caulle, Ranco, Puyehue2/PCC2 and Puyehue1/PCC1 (Figure 8; Fontijn et al., 2016; Lara et al., 2006; Naranjo et al., 2017; Singer et al., 2008), and volcanic actvity during the Deglaciation has been identified by $^{40}Ar/^{39}Ar$ dating of some effusive products between 12 ± 2.8 and 18.7 ± 1.1 cal ka BP (Singer et al., 2008). Finally, two tephras of Yate volcano have been recognized in the literature: Ya1 and Ya2. Ya2 has been dated bracketed between ~0.4 and 0.9 cal ka BP, whereas Ya1 is thought to represent a Holocene eruption but its age is not constrained (Watt et al., 2011b). Additionally, $^{40}Ar/^{38}Ar$ dating together with the observation of volcanic products associated or not with glacial erosion have been identified and ascribed to the Yate volcano, suggesting a continuous activity since 122 ± 19 cal ka BP (Mella, 2008). Geochemically, some differences can be observed between these volcanic centers. When comparing glass shard major elements (Figure 4, Figure S8), Puyehue-Cordón Caulle products are mainly dacitic or rhyolitic (66–74 wt.% SiO2) with relatively intermediate K (2.2–3.5 wt.% K_2O; (Alloway et al., 2015; Fontijn et al., 2016; Naranjo et al., 2017)) compared to the other volcanoes with similar silica concentration (Yate: 2.6–3.5 wt.% K_2O; Antillanca-Casablanca: 2.2–3.2 wt.% K_2O). Antillanca-Casablanca glass shards display a trend with relatively less evolved products (56–75 wt.% SiO_2) than Puyehue-Cordón Caulle, from andesitic to rhyolitic compositions at relatively lower K than Puyehue-Cordón Caulle (Fontijn et al., 2016; Geoffroy et al., 2018; Naranjo et al., 2017; Villarosa et al., 2006). In the case of Yate, individual glass shards ranging from andesites to rhyolites have been erupted since the last glaciation (Mella, 2008; Watt et al., 2011b). The eruption with the most information corresponds to Ya2, which displays a continuous trend from basaltic andesite to rhyolite with relatively higher K than the two other volcanoes (Figure 4a, c, e), particularly at andesitic compositions (Figure 4c, e). For the three volcanic centers, whole–rock compositions (Gerlach et al., 1988; Jacques et al., 2014; Lara et al., 2006; López-Escobar et al., 1993; Mella, 2008; Naranjo et al., 2017; Rawson et al., 2016; Singer et al., 2008) record a more complete trend, from basalts and basaltic andesite to rhyolite, however andesites are rare in Puyehue-Cordón Caulle and Antillanca-Casablanca.

Additionally, these volcanic centers can be distinguished based on their trace elements. Notably, La/Yb values of Puyehue-Cordón Caulle are lower, plotting between 4–7 (Figure 4b), with Zr/Nb values ranging between 22 to 50; meanwhile Antillanca-Casablanca displays very heterogeneous La/Yb values ranging between 4–21 and Zr/Nb values from 21 to 62; and Yate displays La/Yb values between 3–12 and Zr/Nb from 24 to 39. The latter helps discriminate between Puyehue-Cordón Caulle and the other two volcanic centers, however Antillanca-Casablanca and Yate cannot be distinguished based on these ratios. When looking at other trace elements, for example Th versus Zr, Th versus Nb or Ce versus Ta (Figure S10) a similar behavior continues to be observed between Antillanca-Casablanca and Yate, thus at present a robust geochemical discrimination between them is not possible. In the following section, we discuss the potential source and correlative of each cryptotephra based on the available information, which for the moment is mainly associated with eruptions from the Puyehue-Cordón Caulle, however always keeping in mind that future work might reveal new tephras associated with Antillanca-Casablanca and/or Yate.

5.2.1 T1/98

The most recent cryptotephra layer from Group 2, T1/98, occurs in the Late Holocene and has an estimated age of ~0.3 cal ka BP (1σ: 0.4–0.1). T1/98 displays bimodal compositions with two clusters between 54–60 and 66–69 wt.% SiO_2, and its major element geochemistry

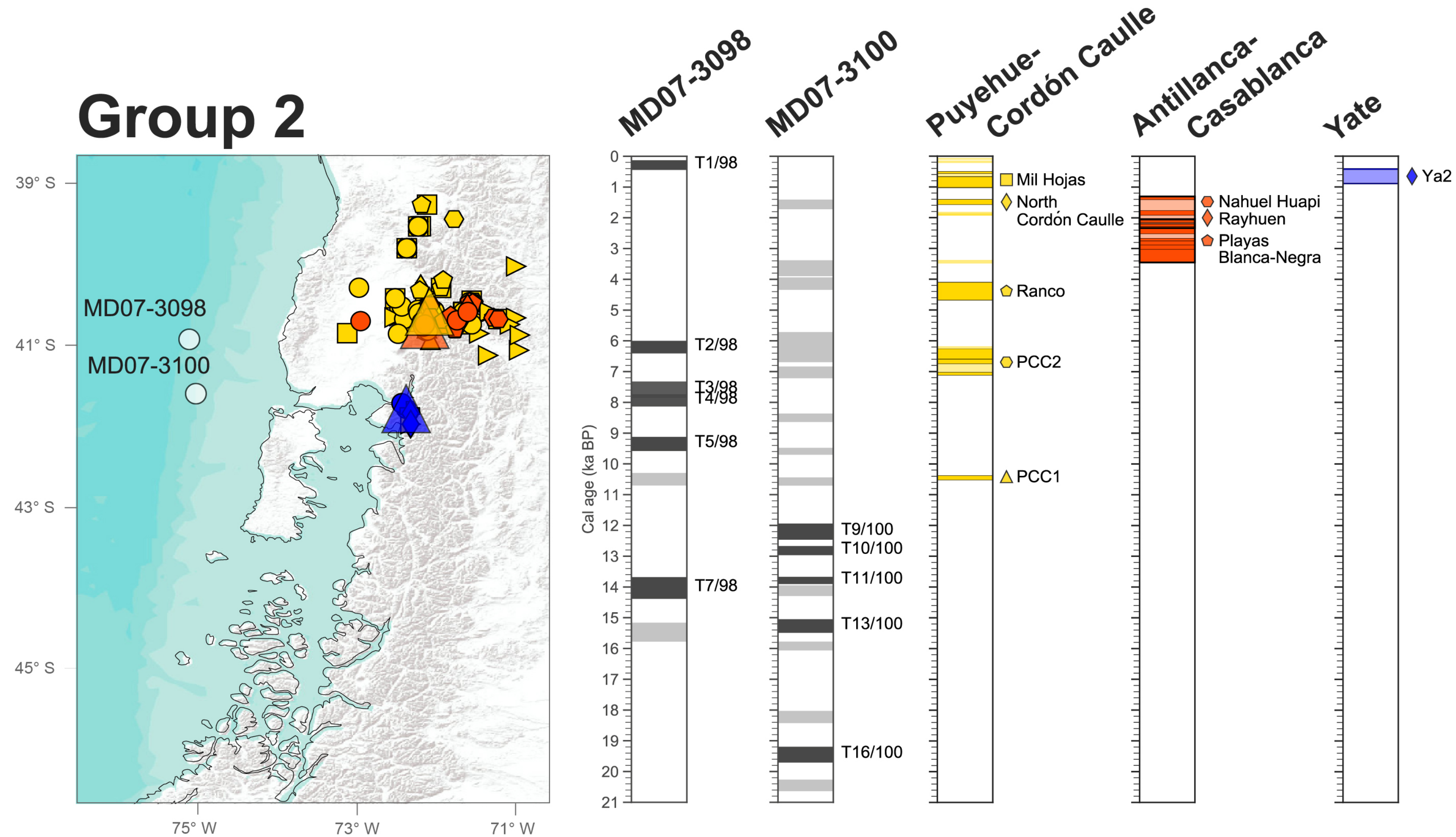

Figure 8. Chronology for cores MD07-3098 and MD07-3100 highlighting the cryptotephra associated to Group 2, as described in the text, compared with the chronologies of explosive products from each volcanic center displaying a similar geochemical behavior (Figure 4). Only events dated by ^{14}C are plotted. To the left: position of the marine sediment cores here studied together with the position of each volcanic center associated to Group 2 indicated as a triangle, from north to south: Puyehue-Cordón Caulle, Antillanca-Casablanca and Yate. Also shown are the position of tephrochronological samples associated with each volcanic center which have been analyzed for geochemistry and/or dated as smaller size symbols. Each symbol corresponds to a different eruptive event indicated to the right in the respective volcanic center chronology (to the right). Pyroclastic deposits which have been dated but no correlation has been stablished are plotted in the chronology but unlabeled and the position is indicated as a dot of the corresponding volcanic center color. Details on the chronologies of each volcanic center in Table S6.

is more consistent with the available information from Yate than that of Puyehue-Cordón Caulle or Antillanca-Casablanca (Figure 4c). Notably, andesitic compositions are frequent in the most primitive glass shards of T1/98, but are virtually absent or very rare in Puyehue-Cordón Caulle and Antillanca-Casablanca volcanic products. Therefore, tephra T1/98 could be a correlative of the most documented eruption from Yate volcano Ya2 (Figure 8), bracketed between ~0.4 and ~0.9 cal ka BP. Additionally, although less likely, it could correspond to a Puyehue-Cordón Caulle eruption, for which many Late Holocene tephras have been described. In particular, the most recent described tephra from Puyehue-Cordón Caulle corresponds to the Mil Hojas eruption, for which an age estimate has been obtained by several authors between ~0.5 and ~1 cal ka BP (Fontijn et al., 2016; Lara et al., 2006; Naranjo et al., 2017; Singer et al., 2008), slightly older than T1/98. Additionally, two pyroclastic density current deposits associated with the Puyehue-Cordón Caulle and younger than Mil Hojas have age estimates of ~0.1 (1σ range: 0.1–0.06) and ~0.2 (1σ range: 0.2–0.1) cal ka BP (Table S6, Lara et al., 2006). At the same time, Naranjo et al. (2017) also recognize two tephra deposits associated to Puyehue-Cordón Caulle which are older than the historic eruption of AD 1921–1922 and younger than the Late Holocene Mil Hojas eruption. It is possible that these deposits are correlated with the pyroclastic density current dated by Lara et al. (2006) and T1/98. Unfortunately, there is no geochemistry available for either of these deposits and thus, a further correlation cannot be done. The most likely correlative of T1/98 would thus be the eruption Ya2 based on available information.

5.2.2 T2/98

T2/98 occurred during the Middle Holocene at an estimated calendar age of 6.2 cal ka BP (1σ: 6.4-6). Around this time, one eruption associated with Puyehue-Cordón Caulle has been described in the literature: Puyehue 2/PCC2, with estimated calendar ages ranging from 6.4 to 7.1 cal ka BP (Fontijn et al., 2016; Lara et al. 2006; Naranjo et al., 2017; Singer et al., 2008). The deposits corresponding to Puyehue 2/PCC2 were first ^{14}C dated by Lara et al. (2006) at ~6.7 (1σ: 6.7–6.6) cal ka BP (Figure 8, Table S6). The same deposit is also described by Singer et al. (2008) who obtained bulk tephra geochemistry for the pyroclastic deposit and whole–rock geochemistry for its effusive correlative, a rhyolite lava dome named Pr2 and dated by $^{40}Ar/^{39}Ar$ in 6.4 ± 0.9 and 6.9 ± 1.6 cal ka BP. Additional information is provided by Fontijn et al. (2016), who obtained individual glass shard major element geochemistry for a likely correlative of this tephra (which they name PCC2), and provide a modelled age of ~6.4 cal ka BP. Finally, Naranjo et al. (2017) date the underlying sediment of this tephra in 7.1 cal ka BP (1σ: 7.2–7). From a chronological point of view it is possible that cryptotephra T2/98 is correlated to Puyehue2/PCC2. From a geochemical point of view, the most evolved cluster from T2/98, with values between ~70–75 wt.% SiO_2 is consistent with analyses of PCC2 (Figure 4d) but the marine tephra follows a more complete trend with SiO_2 values ranging from ~60–75 wt.% SiO_2, whereas on land volcanic products are restricted to 70–73 wt.% SiO_2. However, most of the available analyses were obtained by Fontijn et al. (2016), who mention that less evolved products were sampled but not analyzed because of the highly crystalline ground mass hampering major element measurements. Thus, the lack of less evolved products from Puyehue 2/PCC2 might be an analytical bias rather than a geochemical fingerprint of this eruption.

5.2.3 T3/98 and T4/98

T3/98 occurred during the Middle-Early Holocene with calendar age estimates of ~7.6 cal ka BP (1σ: 7.9–7.3). It displays bimodal compositions with two clusters between 56–59 and 65–72 wt.% SiO_2 (Figure 4e). T4/98 occurred during the Middle-Early Holocene at ~7.9 cal ka BP (1σ: 8.1–7.7). Glass shards in T4/98 display a continuous trend from 59–73 wt.% SiO_2. During this time interval none of the volcanic centers in Group 2 has a recorded activity (Figure 8), except for effusive products of Puyehue-Cordón Caulle dated at 6.9 ± 1.6 ka which have been correlated to the Puyehue2/PCC2 eruption (Singer et al., 2008). From the major elements alone it is not possible to further constrain the volcanic source of either of these two cryptotephra, thus future work might reveal potential correlatives for them.

5.2.4 T5/98

T5/98 occurs in the Early Holocene at ~9.4 cal ka BP (1σ: 9.6–9.1). It presents a bimodal geochemistry with values between 54–61 and 67–72 wt.% SiO_2. The only described eruption from volcanoes in Group 2 during the Early Holocene corresponds to Puyehue 1/PCC1. Puyehue 1/PCC1 is a tephra found overlying moraine deposits or directly on rocks presenting glacial erosion (Naranjo et al., 2017), which has been dated by Singer et al. (2008), as part of unit Pr1, at ~10.5 cal ka BP (1σ: 10.5–10.4) and its whole–rock analysis corresponds to a dacitic composition. The estimated calendar ages of T5/98 and PCC1 do not coincide, notably the estimated calendar age of Puyehue 1/PCC1 is ~1000 years older than that of T5/98. When comparing the major element geochemistry of T5/98 and that of

PCC1/Puyehue 1 (Figure 4f), the most evolved part of the bimodal trend in the marine tephra is coincident with glass shard analyses by Fontijn et al. (2016) and whole–rock analyses by Singer et al. (2008). Additionally, one bulk tephra analysis (Rawson et al., 2016) has values similar to the less evolved part of the trend observed in T5/98, around 61 wt.% SiO_2 (Figure 4f).

With the current age assessment for Puyehue 1/PCC1, it seems unlikely that T5/98 is the correlative of this tephra. However because so far only one age constraint is available, the estimated age of PCC1 might greatly vary in the future. As mentioned, for example, in the case of MIC1 in Section 5.1.4.2, for which the estimated age ranges between ~5.8 and 7.2 cal ka BP, age constraints for a tephra can greatly vary at different sites depending on the measured material and stratigraphic position of it, and thus the assessment of more dates could help further constraint the correlation between Puyehue 1/PCC1 and T5/98.

5.2.5 T9/100

Cryptotephra T9/100, occurring at ~12.2 cal ka BP (1σ: 12.5–11.9), is the only cryptotephra from Group 2 for which trace elements have been analyzed. As mentioned before, volcanoes in Group 2 can be further distinguished based in their La/Yb ratios. In particular, Puyehue-Cordón Caulle has very uniform and relatively low La/Yb values, around 5. In contrast, Antillanca-Casablanca and Yate volcanic centers display more heterogeneous La/Yb values ranging between ~3–21, similar to what is observed in T9/100 which presents values between ~5–12 (Figure 4b). Surprisingly, when looking at other trace element concentrations, such as Th versus Zr or Nb, cryptotephra T9/100 seems to follow a

Puyehue-Cordón Caulle trend (Figure S14). From the latter, the geochemical signature from T9/100 is so far puzzling and a potential source is not yet identifiable.

5.2.6 Deglacial and late glacial cryptotephras

According to our results, five cryptotephras from Group 2 occur during the Deglaciation and one during the late glacial period in addition to T9/100. Cryptotephra T10/100 occurs at ~12.8 cal ka BP (1σ: 13–12.7), T11/100 at ~13.8 cal ka BP (1σ: 13.9–13.7), T7/98 at ~14 cal ka BP (1σ: 14.4–13.7), T13/100 at ~15.3 cal ka BP (1σ: 15.5–15) and finally T16/100 at ~19.4 cal ka BP (1σ: 19.7–19.2). From these, it is possible that T7/98 and T11/100 are correlated since they are within error synchronous and display similar major element trends (Figure 4h, S15).

No tephra deposits have been robustly identified on land for the volcanic centers in Group 2 during the Deglaciation. As previously mentioned, Puyehue1/PCC1 (~10.5 cal ka BP (1σ: 10.5–10.4) is found deposited over moraine deposits or glaciated rocks (Naranjo et al., 2017), hence no older tephra deposit is known. However, Singer et al. (2008) dated effusive products of the Puyehue-Cordón Caulle by $^{40}Ar/^{39}Ar$ at 12 ± 2.8, 12.3 ± 1.9, 14.9 ± 2.9, 18.7 ± 1.1 cal ka BP. Unfortunately, the higher error associated with the $^{40}Ar/^{39}Ar$ method relative to ^{14}C dating does not allow a direct correlation with these products. However, this information demonstrates that Puyehue-Cordón Caulle was active during the Deglaciation and late glacial and thus it is a plausible source for the marine cryptotephras. Additionally, the effusive products from Puyehue-Cordón Caulle follow a wide range from basalts to rhyolites, coherent with the compositional variations found in cryptotephras from Group 2 (Figure 4g).

Further information on the volcanic activity of volcanic centers in Group 2 during the Deglaciation might be found in a lake core record from Lago Puyehue (Pu-II; Bertrand et al., 2008), where two tephra layers with similar geochemistry (PU-II 929–930 and 933–934 cm) have an estimated age slightly older than 13.8 cal ka BP. Bertrand et al. (2008) propose a Puyehue-Cordón Caulle source for PU-II 933–934 cm and suggest a more distant source for PU-II 929–930, however no exact volcanic center is indicated. When observing their major element geochemistry, they both present a bimodal trend with the more evolved part of the trend plotting very closely to the more evolved products from Antillanca-Casablanca and Puyehue-Cordón Caulle (Figure 4h). On the other hand, the less evolved part of the trend could correspond to either of the volcanic centers in Group 2. When comparing these tephras with T11/100 and T7/98, dated at ~13.8 and ~14 cal ka BP respectively, both cryptotephras and tephras on land represent bimodal trends with geochemical similarities around the less evolved clusters at ~60 wt.% SiO_2. However, at higher silica values the comparison between products becomes less consistent, the on land tephras having higher SiO_2 contents for lower K_2O. Thus it is unlikely that they correspond to correlatives.

As a summary for Group 2, eleven cryptotephras were identified as either Puyehue-Cordón Caulle, Antillanca-Casablanca or Yate sourced. However, the paucity of literature information did not enable us to correlate with robustness any of these cryptotephras. We suggest that T1/98 might be correlated to Ya2, and that more on land chronological constraints together with trace element analyses could help further constrain this correlation and better discriminate it from Puyehue-Cordón Caulle activity at this time. Additionally we suggest that T2/98 might be correlated to PCC2/Puyehue 2, if less evolved products from the latter are analyzed; and T5/98 to PCC1/Puyehue 1, if more age constraints on land become available. Regarding the remaining cryptotephras in this group, no tentative correlations could be established. However the data presented here supports previous evidence for volcanic activity of Puyehue-Cordón Caulle and Yate during Holocene, deglacial and late glacial periods for which the marine tephras might represent the distant evidence of this explosive volcanic activity. A better correlation with the on land information however requires more geochronological and geochemical data, for example Ya1 eruption so far no age constraint exits and only two geochemical bulk analyses of the tephra are available (Watt et al., 2011b). Additionally, most deglacial evidence potentially correlated to the cryptotephra here analyzed corresponds to $^{40}Ar/^{39}Ar$ dating in effusive products which does not allow for a correlation because of the high errors associated with $^{40}Ar/^{39}Ar$ dating relative to ^{14}C dating.

5.3 Group 3

Cryptotephra layer T8/98 occurs at the beginning of the Deglaciation and has an estimated calibrated age of ~15.5 cal ka BP (1σ: 15.8–15.2). The major element geochemistry of this cryptotephra is unique in both cores analyzed here, with much lower K_2O values ranging between ~0.5 and 1.3 wt.% at variable SiO_2 contents (Figure 5a and 3a, 4a for comparison). This particular geochemical fingerprint is shared by eight volcanic centers dispersed between 39 and 45° S along the SVZ (Figure 1): Llaima (Bouvet de Maisonneuve et al., 2012; Naranjo and Moreno, 1991, 2005; Rawson et al., 2016; Reubi et al., 2011; Schindlbeck et al., 2014; Lohmar, 2008), Osorno (Bertrand et al., 2008; Jacques et al., 2014; López-Escobar et al., 1993; López-Escobar et al., 1992; Moreno et al., 2010; Tagiri et al., 1993), Calbuco (López-Escobar et al., 1995, 1992; Morgado et al., 2019; Watt et al., 2011b; Sellés and Moreno, 2011), Hornopirén (Watt et al., 2011b), Huequi (Watt et al., 2011a), Corcovado, Yanteles (López-Escobar et al., 1993; Naranjo and Stern, 2004) and Mentolat (López-Escobar et al., 1993; Naranjo and Stern, 2004; Stern et al., 2015; Weller et al., 2019, 2017, 2015).

Among these volcanoes, one eruption from the Llaima volcano has been well described and dated with a similar age to T8/98 (~15.5 cal ka BP). The Curacautín Ignimbrite, resulting from this eruption, is proposed to have occurred in two phases based on ^{14}C ages populations and field observations (Lohmar, 2008): Curacautín 1 (Table S6) with a mean age of ~16.1 cal ka BP and Curacautín 2 with a mean age ~15 cal ka BP (Figure 9). A direct geochemical comparison of individual glass shards major element geochemistry between T8/98 and Curacautín products indicates similar values below 60 wt.% SiO_2 (Figure 5b), however the more evolved values observed in T8/98 with low K_2O are not present in Curacautín, for which glass shards with higher silica values display much higher K than tephra T8/98. The geochemical trend displayed by T8/98 seems more consistent with a poorly described pyroclastic deposit from the Calbuco volcano, dated at ~14.4 cal ka BP (Sellés and Moreno, 2011). For this deposit no geochemical data have been reported and the stratigraphic position of the charcoal used for ^{14}C dating is unknown, hampering further robust correlation. Regarding the remaining volcanoes, no deposits have been identified during this time interval (Figure 9) and the Osorno volcano is thought to be a volcano with a dominant effusive activity (Moreno et al., 2010), it might thus be a less likely possible source for T8/98.

From the latter, it is plausible that the cryptotephra T8/98 is correlated to either Curacautín1, 2 or the unknown event from Calbuco volcano. Given the wind configuration in the area and the position of the volcanic centers relative to core MD07-3098, Calbuco volcano would be the more likely source of the cryptotephra (Figure 1). However, given the chaotic nature of atmospheric circulation as described in section 2, a Llaima source is not impossible.

Further information, especially regarding the volcanic activity of Calbuco could help clarify

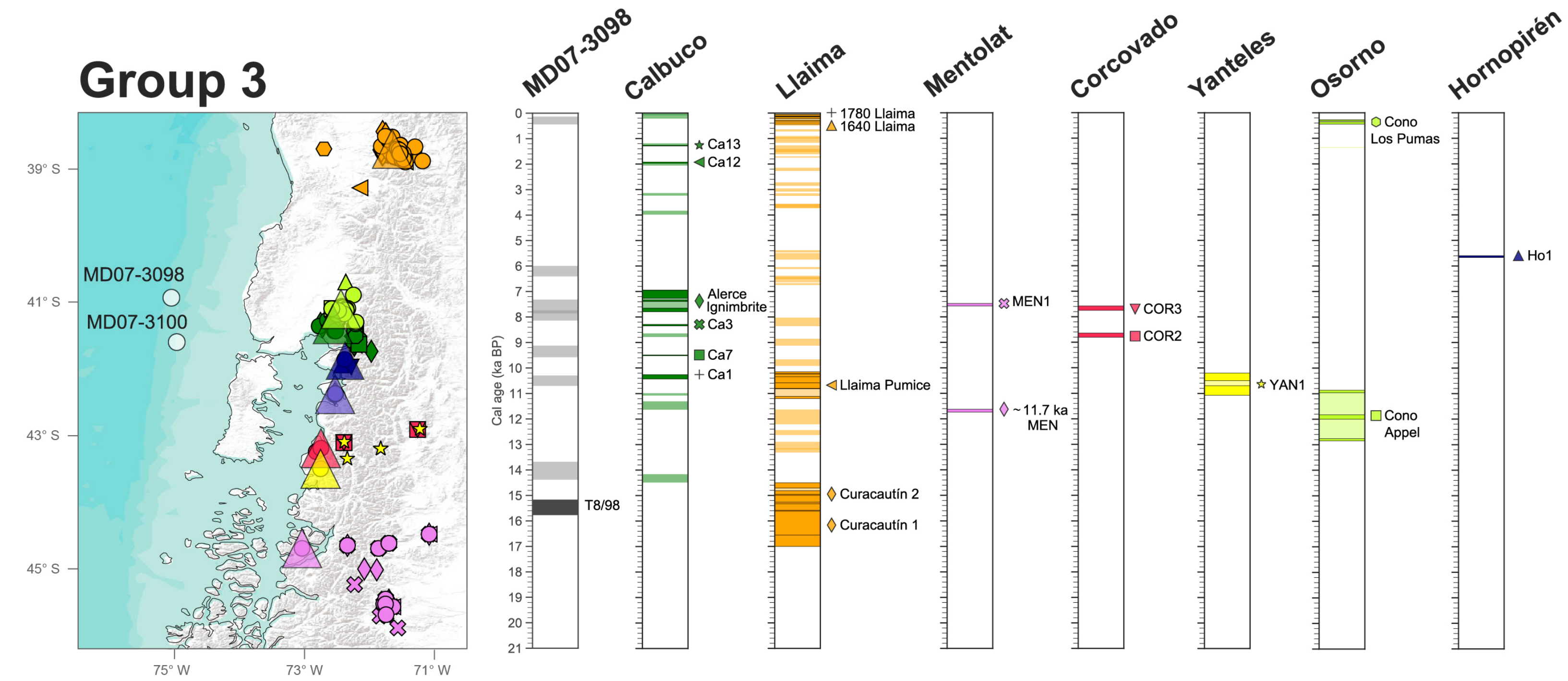

Figure 9. Chronology for cores MD07-3098 and MD07-3100 highlighting the one cryptotephra associated to Group 3 (T8/98), as described in the text, compared with the chronologies of explosive products from each volcanic center displaying a similar geochemical behavior (Figure 6). Only events dated by ^{14}C are plotted. To the left: position of the marine sediment cores here studied together with the position of each volcanic center associated to Group 3 indicated as a triangle, from north to south: Llaima, Osorno, Calbuco, Hornopirén, Huequi (no eruptive events have been dated for Huequi so far), Corcovado, Yanteles and Mentolat. Also shown are the position of tephrochronological samples associated with each volcanic center which have been analyzed for geochemistry and/or dated, as smaller size symbols. Each symbol corresponds to a different eruptive event indicated in the respective volcanic center chronology (to the right). Pyroclastic deposits which have been dated but no correlation has been stablished are plotted but unlabeled in the chronology and the position is indicated as a dot of the corresponding volcanic center color. Details on the chronologies of each volcanic center in Table S6.

this possible correlation in the future.

5.4 General comment

As mentioned in the previous sections, all the cryptotephra and tephra layers analyzed here represent a trend, either bimodal or continuous, from basaltic andesite to dacite or rhyolite, which is in contrast with many records on land which represent clusters. This was also observed by Carel et al. (2011) when comparing marine tephra layers and on land tephras from the Hudson volcano. This difference, which is observed in the case of T2/100 versus LTT-9 and LTT-10, T3/100 versus H2 (Figure 3d, e), T4/100 or T5/100 versus LTT-14 and LTT-15, LTT-20 compared to T6/100 (Figure 7a, c), T2/98 versus Puyehue 2/PCC2 (Figure 4d) might indicate either that the deposits on land and the ocean arise from different eruptive events or it could also arise from biases associated to the dispersion of the ashes and/or measuring techniques. For example, it has been mentioned in the literature that analytical biases arise by the increased difficulty in analyzing glass shards with microlites, which are more abundant in less evolved melts (e.g. Alloway et al., 2017a; Fontijn et al., 2016). The latter could explain the lack of less evolved products in LTT-20 compared to T6/100 (Figure 7c), however it would not explain the differences observed in T2/100 versus LTT-9 and LTT/10 (Figure 3d) and T4/100 or T5/100 versus LTT-14 and LTT-15 (Figure 7a).

An interesting situation regarding this point is observed in both identified eruptions in this study: HW7 and Lepué tephra. For both these tephras a number of different sections have been analyzed for geochemistry on land for which different sections display different geochemistry. In particular, in the case of Lepué tephra, none of the analyzed sections on land represent the whole trend (Alloway et al., 2017a; Amigo et al., 2013), however all marine

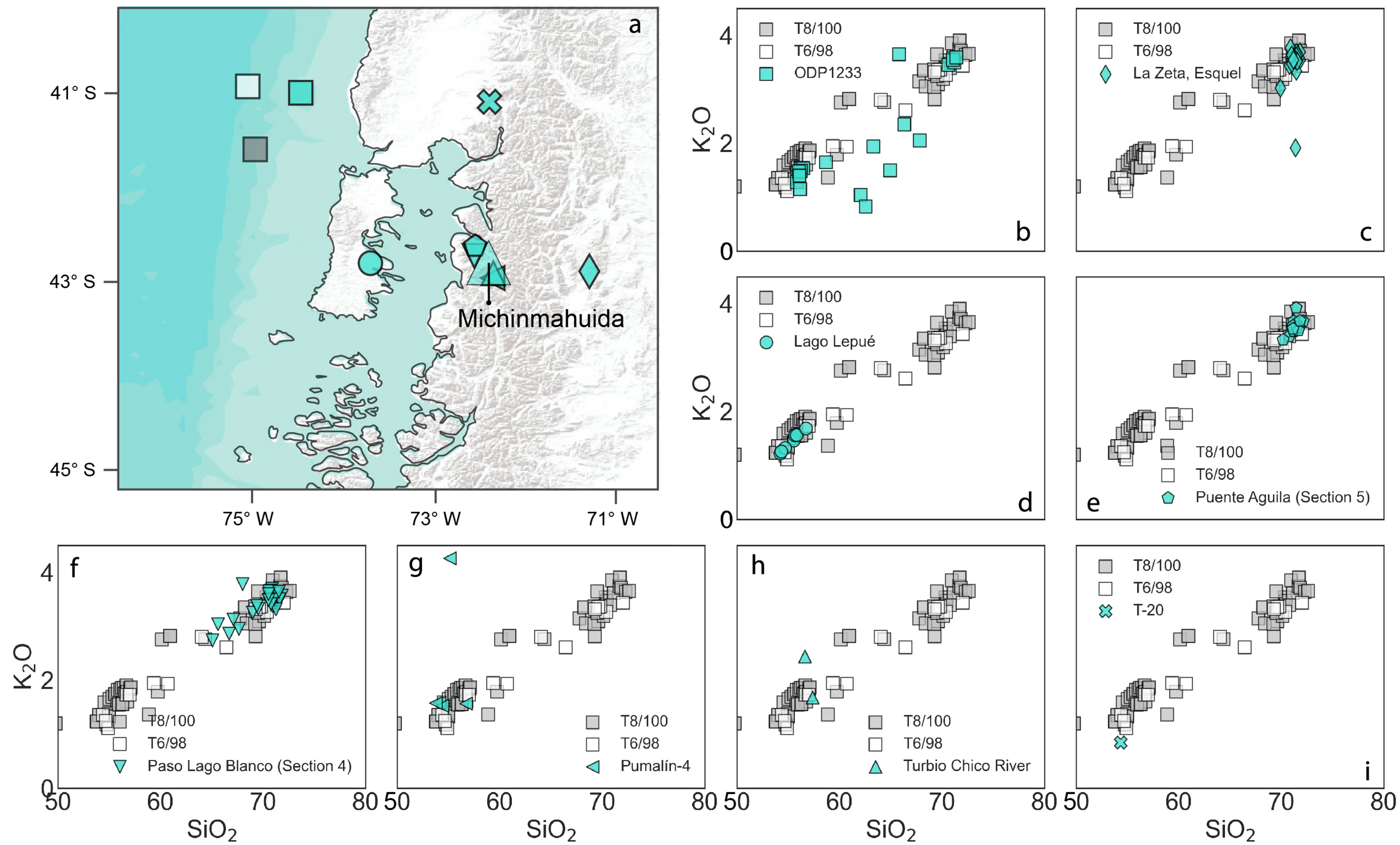

Figure 10. SiO_2 vs K_2O and position (a) of deposits correlated with Lepué tephra), indicated in the legend (b–i) are the given name for each section in which the Lepué tephra was identified and analyzed. b–g deposits analyzed by Alloway et al. (2017a); i: Analyzes of Amarillo ignimbrite, correlative of Lepué tephra (Amigo et al., 2013); h: Analysis of Lepué correlative analyzed by Naranjo & Stern (2004), who initially identified this deposit as COR1.

tephras do, including ODP-202 site 1233 and both tephras here analyzed (Figure 10). In addition, a similar situation is observed for tephra HW7, however in this case two of the studied sections on land: "Laguna Marcelo" and "Laguna Stibnite" also display the full trend (Haberle & Lumley, 1998), as do cryptotephra T1/100 and cryptotephra at 160 cm in core MD07-3088 (Carel et al., 2011), all of them located to the west of Hudson volcano. It is difficult to pinpoint what give rise to the different geochemical compositions in the different sections as this probably arises from a sum of different biases. For example: bias associated with the depositional environment; bias associated with the analytical techniques; biases associated with the very nature of the eruption i.e. its explosiveness and/or duration; and finally, biases associated with the dispersal conditions of their products, such as wind direction at the moment of the eruption. For these various reasons, marine cryptotephra might have the capacity of recording a more complete geochemical trend from a single volcano than on land tephras. Although the reasons are still unclear, this would mean that marine tephras/cryptotephras can thus serve as robust compositional reference for further correlations because they would be less geochemically biased. In addition to the robust stratigraphic constraints here provided for each tephra and cryptotephra, the geochemistry of the marine tephras/cryptotephras constitute robust tephrochronological constraints to disentangle the complex tephrochronological record in the SVZ.

6. Conclusion

Here we present a continuous marine (crypto) tephrochronological record associated with the SVZ, derived from two marine sediment cores retrieved in the Chilean continental margin. From the twenty five tephras and cryptotephras analyzed: one cryptotephra was correlated with tephra HW7 from Hudson volcano previously identified by Carel et al. (2011) and Haberle and Lumley (1998); and the Lepué tephra (Alloway et al., 2017a; Amigo et al., 2013), associated with Michinmahuida volcano, was identified in both studied cores as a ~25–30 cm–thick visible tephra layer. The latter constitutes an important tie point to align not only the chronologies of cores MD07-3098 and MD07-3100, but also the chronologies of other available paleoceanographic record in the area, such as ODP-202 site 1233 (Lamy et al., 2004, 2015) and MD07-3088 (Carel et al., 2011; Siani et al.2013). Thus representing a step forward towards producing a chronologically robust paleoceanographic record in the area.

Additionally, eight cryptotephra were identified as Michinmahuida sourced based on major and trace elements for which robust stratigraphic constraints are provided. The latter is in agreement with previous records suggesting continuous Holocene activity of Michinmahuida (Amigo et al., 2013; Moreno et al., 2014), and provides new and robust evidence for its deglacial and late glacial activity. Eleven cryptotephra were identified as sourced either from Puyehue-Cordón Caulle, Antillanca-Casablanca or Yate, even though no robust correlation could be established at this stage. Nevertheless, they represent evidence for late glacial and deglacial explosive activity of either of these volcanic centers, for which evidence on land has only been previously identified by Bertrand et al. (2008). The latter complements previous information from Puyehue-Cordón Caulle (Singer et al., 2008) and Yate (Mella, 2008) for which effusive products have been dated indicating late glacial and deglacial ages and provides further chronological constraints for the Puyehue-Cordón Caulle activity.

Overall, the marine sediment cores here studied provide robust geochemical and stratigraphic evidence for a continuous volcanic activity in the SVZ since the late glacial (~20 cal ka BP). In the future, this information, together with an increased geochemical and chronological on land database, might help further unveil the volcanic activity of the different volcanic centers and provide additional tie points to synchronize different paleo environmental records in the area.

7. Acknowledgements

We thank the captains and the crew of the R/V Marion Dufresne during the PACHIDERME cruise for their help retrieving cores MD07-3098 and MD07-3100. We would also like to thank the French INSU-LEFE-IMAGO SEPORA project 2016 (2016-2018), the French/Chilean ECOS SUD-CONICYT project C15U04 2016–2019 and the Chilean National Agency of Research and Development (ANID) for their financial support through Becas Chiles, Doctorado en el Extranjero Convocatoria 2017. We are thankful to the French ^{14}C AMS facility ARTEMIS and EchoMicadas for the chemical preparation and measurements of the ^{14}C samples. We also thank Frédéric Haurine for his assistance during laser ablation ICP-MS. Finally we very sincerely thank people from the Chilean Geological Service (SERNAGEOMIN), especially Álvaro Amigo and Virginia Toloza for kindly facilitating details on their published data and whose comments helped improve the manuscript.

8. Data Availability

Datasets related to this article (Table S1-S5) can be found at ____.

9. References

Alloway, B. V., Moreno, P.I., Pearce, N.J.G., De Pol-Holz, R., Henríquez, W.I., Pesce, O.H., Sagredo, E., Villarosa, G., Outes, V., 2017a. Stratigraphy, age and correlation of Lepué Tephra: a widespread c. 11 000 cal a BP marker horizon sourced from the Chaitén Sector of southern Chile. J. Quat. Sci. 32, 795–829. https://doi.org/10.1002/jqs.2976

Alloway, B. V., Pearce, N.J.G., Moreno, P.I., Villarosa, G., Jara, I., De Pol-Holz, R., Outes, V., 2017b. An 18,000 year-long eruptive record from Volcán Chaitén, northwestern Patagonia: Paleoenvironmental and hazard-assessment implications. Quat. Sci. Rev. 168, 151–181. https://doi.org/10.1016/j.quascirev.2017.05.011

Alloway, B. V., Pearce, N.J.G., Villarosa, G., Outes, V., Moreno, P.I., 2015. Multiple melt bodies fed the AD 2011 eruption of Puyehue-Cordón Caulle, Chile. Sci. Rep. 5. https://doi.org/10.1038/srep17589

Amigo, Á., Lara, L.E., Smith, V.C., 2013. Holocene record of large explosive eruptions from Chaitén and Michinmahuida Volcanoes, Chile. Andean Geol. 40, 227–248. https://doi.org/10.5027/andgeov40n2-a03

Anderson, R.F., Ali, S., Bradtmiller, L.I., Nielsen, S.H.H., Fleisher, M.Q., Anderson, B.E., Burckle, L.H., 2009. Wind-driven upwelling in the Southern Ocean and the Deglacial Rise in Atmospheric CO_2. Science 323, 1443–1448. https://doi.org/10.1126/science.1167441

Bertin, L., Moreno, H., Becerril, L., 2018. Peligros del Campo Volcánico Carrán-Los Venados, Región de los Ríos. Servicio Nacional de Geología y Minería, Carta Geológica de Chile, Serie Geológica

Ambiental, 33, 1–90, Santiago.

Bertrand, S., Castiaux, J., Juvigné, E., 2008. Tephrostratigraphy of the late glacial and Holocene sediments of Puyehue Lake (Southern Volcanic Zone, Chile, 40°S). Quat. Res. 70, 343–357. https://doi.org/10.1016/j.yqres.2008.06.001

Bertrand, S., Daga, R., Bedert, R., Fontijn, K., 2014. Deposition of the 2011-2012 Cordón Caulle tephra (Chile, 40°S) in lake sediments: Implications for tephrochronology and volcanology. J. Geophys. Res. Earth Surf. 119, 2555–2573. https://doi.org/10.1002/2014JF003321

Bouvet de Maisonneuve, C., Dungan, M.A., Bachmann, O., Burgisser, A., 2012. Insights into shallow magma storage and crystallization at Volcán Llaima (Andean Southern Volcanic Zone, Chile). J. Volcanol. Geotherm. Res. 211–212, 76–91. https://doi.org/10.1016/j.jvolgeores.2011.09.010

Brahm, R., Parada, M.A., Morgado, E., Contreras, C., McGee, L.E., 2018. Origin of Holocene trachyte lavas of the Quetrupillán volcanic complex, Chile: Examples of residual melts in a rejuvenated crystalline mush reservoir. J. Volcanol. Geotherm. Res. 357, 163–176. https://doi.org/10.1016/j.jvolgeores.2018.04.020

Bucchi, F., Lara, L.E., Gutiérrez, F., 2015. The Carrán-Los Venados volcanic field and its relationship with coeval and nearby polygenetic volcanism in an intra-arc setting. J. Volcanol. Geotherm. Res. 308, 70–81. https://doi.org/10.1016/j.jvolgeores.2015.10.013

Carel, M., Siani, G., Delpech, G., 2011. Tephrostratigraphy of a deep-sea sediment sequence off the south Chilean margin: New insight into the Hudson volcanic activity since the last glacial period. J. Volcanol. Geotherm. Res. 208, 99–111. https://doi.org/10.1016/j.jvolgeores.2011.09.011

Casati, E., D'Amico, M., Šefrna, L., Trombino, L., Tunesi, A., Previtali, F., 2019. Geo-pedological contribution to the reconstruction of Holocene activity of Chaitén volcano (Patagonia, Chile). J. South Am. Earth Sci. 94. https://doi.org/10.1016/j.jsames.2019.102222

Cembrano, J., Lara, L.E., 2009. The link between volcanism and tectonics in the southern volcanic zone of the Chilean Andes: A review. Tectonophysics 471, 96–113. https://doi.org/10.1016/j.tecto.2009.02.038

Davies, B.J., Darvill, C.M., Lovell, H., Bendle, J.M., Dowdeswell, J.A., Fabel, D., García, J.L., Geiger, A., Glasser, N.F., Gheorghiu, D.M., Harrison, S., Hein, A.S., Kaplan, M.R., Martin, J.R.V., Mendelova, M., Palmer, A., Pelto, M., Rodés, Á., Sagredo, E.A., Smedley, R.K., Smellie, J.L., Thorndycraft, V.R., 2020. The evolution of the Patagonian Ice Sheet from 35 ka to the present day (PATICE). Earth-Science Rev. 204. https://doi.org/10.1016/j.earscirev.2020.103152

Del Carlo, P., Di Roberto, A., D'Orazio, M., Petrelli, M., Angioletti, A., Zanchetta, G., Maggi, V., Daga, R., Nazzari, M., Rocchi, S., 2018. Late Glacial-Holocene tephra from southern Patagonia and Tierra del Fuego (Argentina, Chile): A complete textural and geochemical fingerprinting for distal correlations in the Southern Hemisphere. Quat. Sci. Rev. 195, 153–170. https://doi.org/10.1016/j.quascirev.2018.07.028

Dumoulin, J.-P., Comby-Zerbino, C., Delqué-Količ, E., Moreau, C., Caffy, I., Hain, S., Perron, M., Thellier, B., Setti, V., Berthier, B., Beck, L. 2017. Status Report on Sample Preparation Protocols Developed at the LMC14 Laboratory, Saclay, France: From Sample Collection to 14C AMS Measurement. Radiocarbon 59, 713–726. https://doi.org/10.1017/RDC.2016.116

Fontijn, K., Lachowycz, S.M., Rawson, H., Pyle, D.M., Mather, T.A., Naranjo, J.A., Moreno-Roa, H., 2014. Late Quaternary tephrostratigraphy of southern Chile and Argentina. Quat. Sci. Rev. 89, 70–84. https://doi.org/10.1016/j.quascirev.2014.02.007

Fontijn, K., Rawson, H., Van Daele, M., Moernaut, J., Abarzúa, A.M., Heirman, K., Bertrand, S., Pyle, D.M., Mather, T.A., De Batist, M., Naranjo, J.A., Moreno, H., 2016. Synchronisation of sedimentary records using tephra: A postglacial tephrochronological model for the Chilean Lake District. Quat. Sci. Rev. 137, 234–254. https://doi.org/10.1016/j.quascirev.2016.02.015

Gallego, D., Ribera, P., Garcia-Herrera, R., Hernandez, E., Gimeno, L., 2005. A new look for the Southern Hemisphere jet stream. Clim. Dyn. 24, 607–621. https://doi.org/10.1007/s00382-005-0006-7

Geoffroy, C.A., Alloway, B.V., Amigo, Á., Parada, M.A., Gutierrez, F., Castruccio, A., Pearce, N.J.G., Morgado, E., Moreno, P.I., 2018. A widespread compositionally bimodal tephra sourced from Volcán Melimoyu (44°S, Northern Patagonian Andes): Insights into magmatic reservoir processes and opportunities for regional correlation. Quat. Sci. Rev. 200, 141–159. https://doi.org/10.1016/j.quascirev.2018.09.034

Gerlach, D.C., Frey, F.A., Moreno-Roa, H., López-Escobar, L., 1988. Recent Volcanism in the Puyehue–Cordon Caulle Region, Southern Andes, Chile (40.5°S): Petrogenesis of Evolved Lavas. J. Petrol. 29, 333–382. https://doi.org/10.1093/petrology/29.2.333

Haberle, S.G., Lumley, S.H., 1998. Age and origin of tephras recorded in postglacial lake sediments to the west of the southern Andes, 44°S to 47°S. J. Volcanol. Geotherm. Res. 84, 239–256. https://doi.org/10.1016/S0377-0273(98)00037-7

Haddam, N.A., Siani, G., Michel, E., Kaiser, J., Lamy, F., Duchamp-Alphonse, S., Hefter, J., Braconnot, P., Dewilde, F., Isgüder, G., Tisnerat-Laborde, N., Thil, F., Durand, N., Kissel, C., 2018. Changes in latitudinal sea surface temperature gradients along the Southern Chilean margin since the last glacial. Quat. Sci. Rev. 194, 62–76. https://doi.org/10.1016/j.quascirev.2018.06.023

Hickey-Vargas, R.L., Frey, F.A., Gerlach, D.C, 1986. Multiple sources for basaltic arc rocks from the Southern Volcanic Zone of the Andes (34°–41°S): trace element and isotopic evidence for contributions from subducted oceanic crust, mantle, and continental crust. J. Geophys. Res. 91, 5963–5983. https://doi.org/10.1029/JB091iB06p05963

Hickey-Vargas, R.L., Holbik, S., Tormey, D., Frey, F.A., Moreno Roa, H., 2016. Basaltic rocks from the Andean Southern Volcanic Zone: Insights from the comparison of along-strike and small-scale geochemical variations and their sources. Lithos 258–259, 115–132. https://doi.org/10.1016/j.lithos.2016.04.014

Hickey-Vargas, R.L., Moreno Roa, H., López-Escobar, L., Frey, F.A., 1989. Geochemical variations in Andean basaltic and silicic lavas from the Villarrica-Lanin volcanic chain (39.5° S): an evaluation of source heterogeneity, fractional crystallization and crustal assimilation. Contrib. to Mineral. Petrol. 103, 361–386. https://doi.org/10.1007/BF00402922

Hogg, A.G., Heaton, T.J., Hua, Q., Palmer, J.G., Turney, C.S.M., Southon, J., Bayliss, A., Blackwell, P.G., Boswijk, G., Bronk Ramsey, C., Pearson, C., Petchey, F., Reimer, P., Reimer, R., Wacker, L., 2020. SHCal20 Southern Hemisphere Calibration, 0-55,000 Years cal BP. Radiocarbon 62, 759–778. https://doi.org/10.1017/RDC.2020.59

Iglesias, V., Whitlock, C., Bianchi, M.M., Villarosa, G., Outes, V., 2011. Holocene climate variability and environmental history at the Patagonian forest/steppe ecotone: Lago Mosquito (42°29’37.89"S, 71°24’14.57"W) and Laguna del Cóndor (42°20’47.22"S, 71°17’07.62"W). The Holocene 22, 1297–1307. https://doi.org/10.1177/0959683611427330

Jacques, G., Hoernle, K., Gill, J., Wehrmann, H., Bindeman, I., Lara, L.E., 2014. Geochemical variations in the Central Southern Volcanic Zone, Chile (38–43°S): The role of fluids in generating arc magmas. Chem. Geol. 371, 27–45.

https://doi.org/10.1016/j.chemgeo.2014.01.015

Jochum, K.P., Nohl, U., Herwig, K., Lammel, E., Stoll, B. and Hofmann, A.W. 2007. GeoReM: A New Geochemical Database for Reference Materials and Isotopic Standards. Geostandards and Geoanalytical Research, 29: 333-338. https://doi.org/10.1111/j.1751-908X.2005.tb00904.x

Kilian, R., Hohner, M., Biester, H., Wallrabe-Adams, H.J., Stern, C.R. 2003. Holocene peat and lake sediment tephra record from the southernmost Chilean Andes (53-55°S). Rev. Geol. Chile 30, 47–64. http://dx.doi.org/10.4067/S0716-02082003000100002

Kissel, C., 2007. MD 159-PACHIDERME IMAGES XV, cruise report 06.02.07-28.02.07. PlouzanÉ inst. polaire français Paul Émile Victor 1, 84.

Kratzmann, D.J., Carey, S., Scasso, R., Naranjo, J.A., 2008. Compositional variations and magma mixing in the 1991 eruptions of Hudson volcano, Chile. Bull. Volcanol. 71, 419–439. https://doi.org/10.1007/s00445-008-0234-x

Lamy, F., Arz, H.W., Kilian, R., Lange, C.B., Lembke-Jene, L., Wengler, M., Kaiser, J., Baeza-Urrea, O., Hall, I.R., Harada, N., Tiedemann, R., 2015. Glacial reduction and millennial-scale variations in Drake Passage throughflow. Proc. Natl. Acad. Sci. U. S. A. 112, 13496–13501. https://doi.org/10.1073/pnas.1509203112

Lamy, F., Kaiser, J., Ninnemann, U., Hebbeln, D., Arz, H.W., Stoner, J., 2004. Antarctic timing of surface water changes off Chile and Patagonian ice sheet response. Science (80-.). 304, 1959–1962. https://doi.org/10.1126/science.1097863

Lara, L.E., Moreno, H., Naranjo, J.A., Matthews, S., Pérez de Arce, C., 2006. Magmatic evolution of the Puyehue-Cordón Caulle Volcanic Complex (40° S), Southern Andean Volcanic Zone: From shield to unusual rhyolitic fissure volcanism. J. Volcanol. Geotherm. Res. 157, 343–366.

https://doi.org/10.1016/j.jvolgeores.2006.04.010

Lohmar, 2008. Pétrologie des grands dépôts d'ignimbrites des volcans Villarrica (Licán et Pucón) et Llaima (Ignimbrite Curacautín), dans les Andes du Sud (Chili). PhD Thesis, Université Blause Pascal - Clermont Ferrand II, France.

López-Escobar, L., Kilian, R., Kempton, P.D., Tagiri, M., 1993. Petrography and geochemistry of Quaternary rocks from the Southern Volcanic Zone of the Andes between 41°30′ and 46°00′S, Chile. Rev. Geol. Chile 20, 33–55. https://doi.org/10.5027/andgeoV20n1-a04

López-Escobar, L., Parada, M.A., Hickey-Vargas, R.L., Frey, F.A., Kempton, P.D., Moreno, H., 1995. Calbuco Volcano and minor eruptive centers distributed along the Liquiñe-Ofqui Fault Zone, Chile (41°–42° S): contrasting origin of andesitic and basaltic magma in the Southern Volcanic Zone of the Andes. Contrib. to Mineral. Petrol. 119, 345–361. https://doi.org/10.1007/BF00286934

López-Escobar, L., Parada, M.A., Moreno, H., Frey, F.A., Hickey-Vargas, R.L., 1992. A contribution to the petrogenesis of Osorno and Calbuco volcanoes, Southern Andes (41°00'-41°30'S): a comparative study. Rev. Geol. Chile 19, 211–226.

Lougheed, B.C., Obrochta, S.P., 2019. A Rapid, Deterministic Age-Depth Modeling Routine for Geological Sequences With Inherent Depth Uncertainty. Paleoceanogr. Paleoclimatology 34, 122–133. https://doi.org/10.1029/2018PA003457

Menviel, L., Spence, P., Yu, J., Chamberlain, M.A., Matear, R.J., Meissner, K.J., England, M.H., 2018. Southern Hemisphere westerlies as a driver of the early deglacial atmospheric CO_2 rise. Nat. Commun. 9, 1–12. https://doi.org/10.1038/s41467-018-04876-4

Mella, M, 2008. Petrogêneses do complexo vulcânico Yate (42, 30ºS), Andes do Sul, Chile. Tese de

Doutorado, Instituto de Geociências, Universidade de São Paulo, São Paulo. https://doi.org/10.11606/T.44.2009.tde-04032009-091537

Moreau, C., Caffy, I., Comby, C., Delqué-Količ, E., Dumoulin, J.-P., Hain, S., Quiles, A., Setti, V., Souprayen, C., Thellier, B., Vincent, J. 2013. Research and Development of the Artemis 14C AMS Facility: Status Report. Radiocarbon 55, Issue 2, 331–337. https://doi.org/10.1017/S0033822200057441

Moreno, P.I., Alloway, B. V., Villarosa, G., Outes, V., Henríquez, W.I., Pol-Holz, R. De, Pearce, N.J.G., 2014. A past-millennium maximum in postglacial activity from Volcán Chaitén, southern Chile. Geology 43, 47–50. https://doi.org/10.1130/G36248.1

Moreno, H., Lara, L., Orozco, G., 2010. Geología del Volcán Osorno, Región de Los Lagos. Servicio Nacional de Geología y Minería, Carta Geológica de Chile, Serie Geológica Básica, 126, 1–31, Santiago.

Moreno, H., Naranjo, J., 2002. Mapa de Peligros del Volcán Llaima, Región de La Araucanía. Servicio Nacional de Geología y Minería, Carta Geológica de Chile, Serie Geología Ambiental 7. Santiago. https://doi.org/10.13140/RG.2.1.1844.3124

Morgado, E., Morgan, D.J., Harvey, J., Parada, M.Á., Castruccio, A., Brahm, R., Gutiérrez, F., Georgiev, B., Hammond, S.J., 2019. Localised heating and intensive magmatic conditions prior to the 22–23 April 2015 Calbuco volcano eruption (Southern Chile). Bull. Volcanol. 81. https://doi.org/10.1007/s00445-019-1280-2

Morgado, E., Parada, M.A., Contreras, C., Castruccio, A., Gutiérrez, F., McGee, L.E., 2015. Contrasting records from mantle to surface of Holocene lavas of two nearby arc volcanic complexes: Caburgua-Huelemolle Small Eruptive Centers and Villarrica Volcano, Southern

Chile. J. Volcanol. Geotherm. Res. 306, 1–16. https://doi.org/10.1016/j.jvolgeores.2015.09.023

Naranjo, J.A., Moreno, H., 1991. Actividad explosiva postglacial en el volcan Llaima, Andes del Sur (38° 45'S). Rev. geol. Chile 18, 69–80. https://doi.org/10.5027/andgeoV18n1-a06

Naranjo, J.A., Moreno, H., Banks, N.G., 1993. La erupción del volcán Hudson en 1991 (46°S), Región XI, Aisén, Chile. Serv. Nac. Geología y Minería Bol. 44, 1–50.

Naranjo, J.A., Moreno, H., 2005. Geología del Volcán Llaima, Región de la Araucanía. Servicio Nacional de Geología y Minería, Carta Geológia de Chile, Serie Geología Básica, 88, 1-33, Escala 1:50.000, Santiago.

Naranjo, J.A., Singer, B.S., Jicha, B.R., Moreno, H., Lara, L.E., 2017. Holocene tephra succession of Puyehue-Cordón Caulle and Antillanca/Casablanca volcanic complexes, southern Andes (40–41°S). J. Volcanol. Geotherm. Res. 332, 109–128. https://doi.org/10.1016/j.jvolgeores.2016.11.017

Naranjo, J.A., Stern, C.R., 2004. Holocene tephrochronology of the southernmost part (42°30'-45°S) of the Andean Southern Volcanic Zone. Rev. Geol. Chile 31, 225–240. https://doi.org/10.4067/S0716-02082004000200003

Naranjo, J.A., Stern, C.R., 1998. Holocene explosive activity of Hudson Volcano, southern Andes. Bull. Volcanol. 59, 291–306. https://doi.org/10.1007/s004450050193

Peccerillo, A., Taylor, S.R., 1976. Geochemistry of Eocene Calc-Alkaline Volcanic Rocks from the Kastamonu Area, Northern Turkey. Contrib. to Mineral. Petrol. 58, 63–81. https://doi.org/10.1007/BF00384745

Pérez-Santos, I., Seguel, R., Schneider, W., Linford, P., Donoso, D., Navarro, E., Amaya-Cárcamo, C., Pinilla, E., Daneri, G., 2019. Synoptic-scale variability of surface winds and ocean response to atmospheric forcing in the eastern austral Pacific Ocean. Ocean Sci. 15, 1247–1266. https://doi.org/10.5194/os-15-1247-2019

Rahn, D.A., Garreaud, R.D., 2014. A synoptic climatology of the near-surface wind along the west coast of South America. Int. J. Climatol. 34, 780–792. https://doi.org/10.1002/joc.3724

Rawson, H., Keller, T., Fontijn, K., Pyle, D.M., Mather, T.A., Smith, V.C., Naranjo, J.A., 2016. Compositional variability in mafic arc magmas over short spatial and temporal scales: Evidence for the signature of mantle reactive melt channels. Earth Planet. Sci. Lett. 456, 66–77. https://doi.org/10.1016/j.epsl.2016.09.056

Rawson, H., Naranjo, J.A., Smith, V.C., Fontijn, K., Pyle, D.M., Mather, T.A., Moreno, H., 2015. The frequency and magnitude of post-glacial explosive eruptions at Volcán Mocho-Choshuenco, southern Chile. J. Volcanol. Geotherm. Res. 299, 103–129. https://doi.org/10.1016/j.jvolgeores.2015.04.003

Reubi, O., Bourdon, B., Dungan, M.A., Koornneef, J.M., Sellés, D., Langmuir, C.H., Aciego, S., 2011. Assimilation of the plutonic roots of the Andean arc controls variations in U-series disequilibria at Volcan Llaima, Chile. Earth Planet. Sci. Lett. 303, 37–47. https://doi.org/10.1016/j.epsl.2010.12.018

Romero, J.E., Morgavi, D., Arzilli, F., Daga, R., Caselli, A., Reckziegel, F., Viramonte, J., Díaz-Alvarado, J., Polacci, M., Burton, M., Perugini, D., 2016. Eruption dynamics of the 22–23 April 2015 Calbuco Volcano (Southern Chile): Analyses of tephra fall deposits. J. Volcanol. Geotherm. Res. 317, 15–29. https://doi.org/10.1016/j.jvolgeores.2016.02.027

Schindlbeck, J.C., Freundt, A., Kutterolf, S., 2014. Major changes in the post-glacial evolution of magmatic compositions and pre-eruptive conditions of Llaima Volcano, Andean Southern

Volcanic Zone, Chile. Bull. Volcanol. 76, 1–22. https://doi.org/10.1007/s00445-014-0830-x

Sellés, D., Moreno, H., 2011. Geología del Volcán Calbuco. Servicio Nacional de Geología y Minería, Carta Geológica de Chile, Serie Geológica Básica, 130, Escala 1:50.000, Santiago.

Sellés, D., Rodríguez, A.C., Dungan, M.A., Naranjo, J.A., Gardeweg, M., 2004. Geochemistry of Nevado de Longaví Volcano (36.2°S): a compositionally atypical arc volcano in the Southern Volcanic Zone of the Andes. Rev. Geol. Chile 31, 293–315. https://doi.org/10.4067/S0716-02082004000200008

Siani, G., Michel, E., De Pol-Holz, R., DeVries, T., Lamy, F., Carel, M., Isguder, G., Dewilde, F., Lourantou, A., 2013. Carbon isotope records reveal precise timing of enhanced Southern Ocean upwelling during the last deglaciation. Nat. Commun. 4. https://doi.org/10.1038/ncomms3758

Singer, B.S., Jicha, B.R., Harper, M.A., Naranjo, J.A., Lara, L.E., Moreno, H., 2008. Eruptive history, geochronology, and magmatic evolution of the Puyehue-Cordón Caulle volcanic complex, Chile. Bull. Geol. Soc. Am. 120, 599–618. https://doi.org/10.1130/B26276.1

Simmons, I.C., McGarvie, D., Cortés, J.A., Calder, E.S., Pavez, A. 2020. Holocene volcanism at the Quetrupillán Volcanic Complex (39°30’ S, 71°43’ W), southern Chile. Volcania, 3(1), pp. 115–137. doi: 10.30909/vol.03.01.115137

Smith, R.E., Smith, V.C., Fontijn, K., Gebhardt, A.C., Wastegård, S., Zolitschka, B., Ohlendorf, C., Stern, C., Mayr, C., 2019. Refining the Late Quaternary tephrochronology for southern South America using the Laguna Potrok Aike sedimentary record. Quat. Sci. Rev. 218, 137–156. https://doi.org/10.1016/j.quascirev.2019.06.001

Stern, C.R., 2004. Active Andean volcanism: its geologic and tectonic setting. Rev. Geol. Chile 31, 161–206. http://dx.doi.org/10.4067/S0716-02082004000200001

Stern, C.R., 2008. Holocene tephrochronology record of large explosive eruptions in the southernmost Patagonian Andes. Bull. Volcanol. 70, 435–454. https://doi.org/10.1007/s00445-007-0148-z

Stern, C.R., De Porras, M.E., Maldonado, A., 2015. Tephrochronology of the upper Río Cisnes valley (44°S), southern Chile. Andean Geol. 42, 173–189. https://doi.org/10.5027/andgeoV42n2-a02

Stuiver, M., Polach, H.A., 1977. Discussion: Reporting of ^{14}C Data. Radiocarbon 19, 355–363. https://doi.org/10.1017/S0033822200003672

Tagiri, M., Moreno, H., López-Escobar, L., Notsu, K. 1993. Two magma types of the high-alumina basalt series of Osorno, Souther Andes (41°06'S)-plagioclase dilution effect. J. Min. Petr. Econ. Geol. 88, 359–371. https://doi.org/10.2465/ganko.88.359

Tisnérat-Laborde N, Thil F, Synal H-A, Cersoy S, Hatté C, Gauthier C, Massault M, Michelot J-L, Noret A, Siani G. et al. 2015. ECHoMICADAS: A new compact AMS system to measuring 14C for environment, climate and human sciences. Paper presented at the 22nd International Radiocarbon Conference. Dakar, Senegal. p. 16–20.

Toggweiler, J.R., Russell, J.L., Carson, S.R., 2006. Midlatitude westerlies, atmospheric CO_2, and climate change during the ice ages. Paleoceanography 21. https://doi.org/10.1029/2005PA001154

Villarosa, G., Outes, V., Hajduk, A., Crivelli Montero, E., Sellés, D., Fernández, M., Crivelli, E., 2006. Explosive volcanism during the Holocene in the Upper Limay River Basin: The effects of ashfalls on human societies, Northern Patagonia, Argentina. Quat. Int. 158, 44–57.

https://doi.org/10.1016/j.quaint.2006.05.016

Wacker, L., Fahrni, S.M., Hajdas, I., Molnar, M., Synal, H.A., Szidat, S., Zhang, Y.L., 2013. A versatile gas interface for routine radiocarbon analysis with a gas ion source. Nucl. Instruments Methods Phys. Res. Sect. B Beam Interact. with Mater. Atoms 294, 315–319. https://doi.org/10.1016/j.nimb.2012.02.009

Watt, S.F.L., Pyle, D.M., Mather, T.A., 2013. Evidence of mid- to late-Holocene explosive rhyolitic eruptions from Chaitén Volcano, Chile. Andean Geol. 40, 216–226. https://doi.org/10.5027/andgeoV40n2-a02

Watt, S.F.L., Pyle, D.M., Mather, T.A., 2011a. Geology, petrology and geochemistry of the dome complex of Huequi volcano, southern Chile. Andean Geol. 38, 335–348. https://doi.org/10.5027/andgeov38n2-a05

Watt, S.F.L., Pyle, D.M., Mather, T.A., Martin, R.S., Matthews, N.E., 2009. Fallout and distribution of volcanic ash over Argentina following the May 2008 explosive eruption of Chaitén, Chile. J. Geophys. Res. Solid Earth 114, 1–11. https://doi.org/10.1029/2008JB006219

Watt, S.F.L., Pyle, D.M., Naranjo, J.A., Rosqvist, G., Mella, M., Mather, T.A., Moreno, H., 2011b. Holocene tephrochronology of the Hualaihue region (Andean southern volcanic zone, ∼42° S), southern Chile. Quat. Int. 246, 324–343. https://doi.org/10.1016/j.quaint.2011.05.029

Weller, D., Miranda, C.G., Moreno, P.I., Villa-Martínez, R., Stern, C.R., 2014. The large late-glacial Ho eruption of the Hudson volcano, southern Chile. Bull. Volcanol. 76, 1–18. https://doi.org/10.1007/s00445-014-0831-9

Weller, D.J., de Porras, M.E., Maldonado, A., Méndez, C., Stern, C.R., 2019. Petrology, geochemistry, and correlation of tephra deposits from a large early-Holocene eruption of Mentolat volcano, southern Chile. J. South Am. Earth Sci. 90, 282–295. https://doi.org/10.1016/j.jsames.2018.12.020

Weller, D.J., De Porras, M.E., Maldonado, A., Méndez, C., Stern, C.R., 2017. Holocene tephrochronology of the lower Río Cisnes valley, souhern Chile. Andean Geol. 44, 229–248. https://doi.org/10.5027/andgeov44n3-a01

Weller, D.J., Miranda, C.G., Moreno, P.I., Villa-Martínez, R., Stern, C.R., 2015. Tephrochronology of the southernmost Andean Southern Volcanic Zone, Chile. Bull. Volcanol. 77, 1–24. https://doi.org/10.1007/s00445-015-0991-2